Chemical Science

ROYAL SOCIETY OF CHEMISTRY

EDGE ARTICLE

View Article Online
View Journal | View Issue

Cite this: *Chem. Sci.*, 2022, **13**, 13748

All publication charges for this article have been paid for by the Royal Society of Chemistry

Received 2nd August 2022
Accepted 31st October 2022

DOI: 10.1039/d2sc04302e

rsc.li/chemical-science

Uranium(IV) alkyl cations: synthesis, structures, comparison with thorium(IV) analogues, and the influence of arene-coordination on thermal stability and ethylene polymerization activity†‡

Nicholas R. Andreychuk,[a] Balamurugan Vidjayacoumar,[a] Jeffrey S. Price,[a] Sophie Kervazo,[b] Craig A. Peeples,[c] David J. H. Emslie, *[a] Valérie Vallet, *[b] André S. P. Gomes,[b] Florent Réal,[b] Georg Schreckenbach, *[c] Paul W. Ayers, *[a] Ignacio Vargas-Baca,[a] Hilary A. Jenkins[a] and James F. Britten[a]

Reaction of $[(XA_2)U(CH_2SiMe_3)_2]$ (**1**; XA_2 = 4,5-bis(2,6-diisopropylanilido)-2,7-di-*tert*-butyl-9,9-dimethylxanthene) with 1 equivalent of $[Ph_3C][B(C_6F_5)_4]$ in arene solvents afforded the arene-coordinated uranium alkyl cations, $[(XA_2)U(CH_2SiMe_3)(\eta^n\text{-arene})][B(C_6F_5)_4]$ {arene = benzene (**2**), toluene (**3**), bromobenzene (**4**) and fluorobenzene (**5**)}. Compounds **2**, **3**, and **5** were crystallographically characterized, and in all cases the arene is π-coordinated. Solution NMR studies of **2**–**5** suggest that the binding preferences of the $[(XA_2)U(CH_2SiMe_3)]^+$ cation follow the order: toluene ≈ benzene > bromobenzene > fluorobenzene. Compounds **2**–**4** generated in C_6H_5R (R = H, Me or Br, respectively) showed no polymerization activity under 1 atm of ethylene. By contrast, **5** and **5-Th** (the thorium analogue of **5**) in fluorobenzene at 20 and 70 °C achieved ethylene polymerization activities between 16 800 and 139 200 g mol^{-1} h^{-1} atm^{-1}, highlighting the extent to which common arene solvents such as toluene can suppress ethylene polymerization activity in sterically open f-element complexes. However, activation of $[(XA_2)An(CH_2SiMe_3)_2]$ {M = U (**1**) or Th (**1-Th**)} with $[Ph_3C][B(C_6F_5)_4]$ in *n*-alkane solvents did not afford an active polymerization catalyst due to catalyst decomposition, illustrating the critical role of PhX (X = H, Me, Br or F) coordination for alkyl cation stabilization. Gas phase DFT calculations, including fragment interaction calculations with energy decomposition and ETS-NOCV analysis, were carried out on the cationic portion of **2′-Th**, **2′**, **3′** and **5′** (analogues of **2-Th**, **2**, **3** and **5** with hydrogen atoms in place of ligand backbone methyl and *tert*-butyl groups), providing insight into the nature of actinide–arene bonding, which decreases in strength in the order **2′-Th** > **2′** ≈ **3′** > **5′**.

Introduction

Cationic early transition metal and f-element alkyl complexes for solution ethylene polymerization are typically generated by reaction of a neutral dialkyl complex (isolated, or generated *in situ*) with a strong electrophile such as $[CPh_3][B(C_6F_5)_4]$, $[HNMe_2Ph][B(C_6F_5)_4]$, $B(C_6F_5)_3$ or methylaluminoxane (MAO), with subsequent polymerization achieved by repeated ethylene coordination and 1,2-insertion steps.[1,2] These activation and polymerization reactions are commonly conducted in arene or alkane solvents; the former is standard in academic laboratories,[3] while the latter is often favored in industry.[4–7] However, olefin polymerization catalysts are frequently generated *in situ* without isolation and characterization. Therefore, the nature and impact of arene solvent coordination is not well explored, and only a handful of early transition metal or f-element alkyl cations which exist as arene-solvent-separated ion pairs have been isolated; crystallographically-characterized examples are shown in Fig. 1.

The arene in $[(Cp^{TMS2})HfMe_2(\eta^6\text{-toluene})][MeB(C_6F_5)_3]$ {Cp^{TMS2} = 1,3-$C_5H_3(SiMe_3)_2$} (**a** in Fig. 1), and the zirconium analogue, is tightly coordinated, as evidenced by a lack of exchange between free and bound toluene on the NMR timescale.[8] Similar metal–

[a]*Department of Chemistry, McMaster University, 1280 Main St. West, Hamilton, L8S 4M1, Ontario, Canada. E-mail: emslied@mcmaster.ca*

[b]*Université Lille, UMR 8523 – Physique des Lasers Atoms et Molecules, F-59000 Lille, France. E-mail: valerie.vallet@univ-lille.fr*

[c]*Department of Chemistry, University of Manitoba, Winnipeg, R3T 2N2, Manitoba, Canada. E-mail: schrecke@cc.umanitoba.ca*

† Dedicated to Prof. Gary J. Schrobilgen for 50 years of outstanding contributions to fundamental Inorganic Chemistry.

‡ Electronic supplementary information (ESI) available: NMR spectra, X-ray crystal structure of $[(XA_2)U(CH_2Ph)_2]\cdot THF$ (**6**·THF), GPC data, representative DSC data, and computational data. CCDC 1848272–1848275 contain the supplementary crystallographic data for **2**, **3**, **5** and **6**, respectively. For ESI and crystallographic data in CIF or other electronic format see DOI: https://doi.org/10.1039/d2sc04302e

arene binding was observed in [Cp*MMe_2(η^6-toluene)][$MeB(C_6F_5)_3$] {M = Hf (**b** in Fig. 1) and Zr}, whereas coordinated toluene is more labile in the titanium analogue.[9,10] Nevertheless, both the titanium [Cp*TiR_3] (R = Me or Bn) compounds and their heavier congeners [Cp*MR_3] (M = Zr, R = Me or Bn; M = Hf, R = Me) were reported to exhibit appreciable ethylene polymerization activity when combined with $B(C_6F_5)_3$ in toluene.[11,12]

The mesitylene-coordinated scandium cation (**c** in Fig. 1), was shown to be an active ethylene polymerization catalyst in bromobenzene, but achieved negligible activity in more-donating toluene, highlighting the impact of arene coordination on polymerization activity.[13,14] McConville *et al.* also proposed arene-coordinated [{$CH_2(CH_2NAr)_2$}TiR(η^6-toluene)]$^+$ {Ar = *o*-xylyl or $C_6H_3{}^iPr_2$-2,6} cations to explain greatly reduced α-olefin polymerization activities in the presence of toluene.[15,16] By contrast, toluene in [{*t*BuNSiMe_2(η^5,η^1-$C_5Me_3CH_2$)}Ti(toluene)]-[$B(C_6F_5)_4$] is only weakly bound in solution, and this compound is highly active for ethylene (1 atm) polymerization in toluene.[17]

The thorium[19,21] and zirconium[18] 4,5-bis(anilido)xanthene complexes (**d–f** in Fig. 1) were reported by one of us (Emslie *et al.*). In the toluene-coordinated trimethylsilylmethyl thorium complex, toluene is not displaced to any significant extent in bromobenzene (in the presence of 5 equiv. of free toluene), and free and coordinated toluene only undergo slow exchange on the NMR timescale at room temperature. In the solid state, the Th–$arene_{centroid}$ distances in [(XA_2)Th(CH_2SiMe_3)(η^6-benzene)][$B(C_6F_5)_4$] and [(XA_2)Th(CH_2Ph)(η^6-toluene)][$B(C_6F_5)_4$] {XA_2 = 4,5-bis(2,6-diisopropylanilido)-2,7-di-*tert*-butyl-9,9-dimethylxanthene} are 2.95 and 2.94 Å, respectively, and the thorium cations are inactive for ethylene (1 atm) polymerization in benzene and toluene. By contrast, toluene in [(XN_2)ZrMe(η^6-toluene)][$B(C_6F_5)_4$] {XN_2 = 4,5-bis(2,4,6-triisopropylanilido)-2,7-di-*tert*-butyl-9,9-dimethylxanthene} is substantially displaced in bromobenzene, even in the presence of 10 equiv. of toluene, and free and coordinated toluene undergo rapid exchange at room temperature. Consistent with more facile toluene displacement, the zirconium complexes are highly active ethylene (1 atm) polymerization catalysts in both toluene and bromobenzene (max. 883 000 g mol^{-1} atm^{-1} h^{-1}). The potential for tetraarylborate counteranions, especially BPh_4^-, to π-coordinate to early transition metal or f-element alkyl species, and the impact of this coordination on olefin polymerization, has also been discussed.[22–28]

Herein we describe the synthesis of a series of uranium cations, [(XA_2)U(CH_2SiMe_3)(η^n-arene)][$B(C_6F_5)_4$] {arene = benzene, toluene, bromobenzene and fluorobenzene}, and crystallographic characterization of the benzene, toluene and fluorobenzene complexes; the latter is the first example of an f-element π-coordinated to a fluoroarene. We also evaluate the ethylene (1 atm) polymerization activity of the uranium(IV) alkyl cations, and their thorium(IV) analogues, generated in a range of solvents including toluene, bromobenzene, *n*-alkanes and fluorobenzene. Furthermore, we describe computational studies on several of the arene-coordinated uranium and thorium alkyl cations, providing insight into the nature and relative strength of actinide-arene π-coordination.

To date, the majority of molecular actinide ethylene polymerization catalysts[29] are metallocene and *ansa*-metallocene complexes, such as [Cp^*_2][ThMe][WCA] (WCA = weakly-coordinating anion, often a tetra(aryl)borate), largely developed by Marks and co-workers.[30–37] For example, [Cp^*_2ThMe][$B(C_6F_4TBS\text{-}p)_4$] (TBS = *tert*-butyldimethylsilyl) achieved a high activity of 920 000 g mol^{-1} h^{-1} atm^{-1} in toluene.[30] However, actinide ethylene polymerization catalysts supported by non-carbocyclic ancillary ligands have also recently emerged.[38] For example, Eisen and co-workers reported the bis(amidinate) actinide(IV) chloro complexes [(2-pyridylamidinate)$_2$AnCl(μ-Cl)$_2$Li(TMEDA)] (2-pyridylamidinate = {$(Me_3SiN)_2C$(2-py)}; An = Th, U) which upon activation with MAO, [CPh_3][$B(C_6F_5)_4$] and/or $Al(^iBu)_3$, produced polyethylene with activities ranging from 100 to 10 000 g mol^{-1} h^{-1} atm^{-1}.[39] However, the active species were not isolated or spectroscopically investigated. Additionally, Leznoff and co-workers reported a variety of neutral uranium(IV) dialkyl complexes,[40] [{κ^3-$(ArNCH_2CH_2)_2O$}U(CH_2R)$_2$] (Ar = 2,6-$^iPr_2C_6H_3$; R = $SiMe_3$, Ph), [(^{tBu}NON)U(CH_2SiMe_3)$_2$], and dimeric [(^{tBu}NON)U{CH($SiMe_3$)($SiMe_2CH_2$)}]$_2$ (^{tBu}NON = {(^{t}BuNSiMe_2)$_2$O}), supported by flexible pincer ligands that achieved ethylene polymerization activities of 20–600 g mol^{-1} h^{-1} atm^{-1} in hexane.

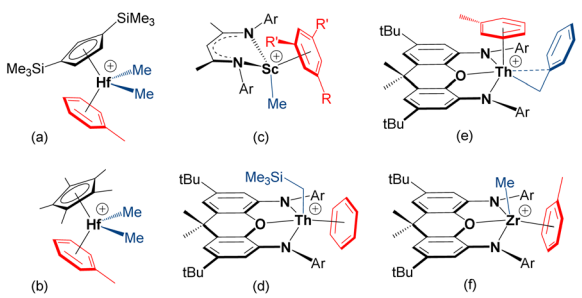

Fig. 1 Crystallographically-characterized early transition metal and f-element alkyl cations which exist as arene-solvent-separated ion pairs (R = Me or Br and R′ = H, or R = R′ = Me; Ar = $C_6H_3{}^iPr_2$-2,6 or $C_6H_2{}^iPr_3$-2,4,6).[8,10,13,14,18–20]

Results and discussion

Experimental studies

Reaction of orange-red [(XA_2)U(CH_2SiMe_3)$_2$] (**1**)[41] with 1 equiv. of [Ph_3C][$B(C_6F_5)_4$] in benzene or toluene afforded the uranium alkyl cations, [(XA_2)U(CH_2SiMe_3)(η^n-arene)][$B(C_6F_5)_4$]·2(arene) {η^n-arene = η^6-benzene (**2**) and η^3-toluene (**3**)} (Scheme 1), which were obtained as deep brown crystals in over 70% yield after crystallization from benzene or toluene layered with hexanes at −30 °C.

In the solid state, **2** exists as a solvent-separated ion pair in which the uranium(IV) monoalkyl cation is stabilized by η^6-coordination to benzene (Fig. 2). Cation **2** has approximate C_s symmetry (with the plane of symmetry bisecting opposing C–C bonds in coordinated benzene) and structurally resembles the neutral dialkyl precursor [(XA_2)U(CH_2SiMe_3)$_2$] (**1**), but with the trimethylsilylmethyl anion in the plane of the XA_2 ligand

replaced by benzene. If the arene in **2** is viewed as the occupant of a single coordination site, uranium adopts a pseudo square-pyramidal geometry with the trimethylsilylmethyl ligand in the apical position. This structure is similar to that of $[(XA_2)Th(CH_2SiMe_3)(\eta^6\text{-}C_6H_6)][B(C_6F_5)_4]$ (**2-Th**),[19] but: (a) the benzene ligand in **2** is rotated by 30° (the plane of symmetry in **2-Th** runs through two of the benzene carbon atoms), and (b) the An–N, An–O, and An–C_{alkyl} distances in **2** are shorter due to the smaller ionic radius of uranium(IV) *versus* thorium(IV) (0.89 *vs.* 0.94 Å for a coordination number of 6).[42] Additionally, the ligand backbone is less planar in **2** in order to accommodate a shorter N(1)···N(2) distance, and the O–An–C_{alkyl} angle is slightly more acute {87.22(9) in **2** *vs.* 91.3(1)° in **2-Th**}, reflecting increased steric hindrance around the smaller actinide metal.

The bonds between uranium and the XA_2 ligand in cationic **2** are 0.03–0.06 Å shorter than those in neutral **1**. By contrast, the U–C_{alkyl} distance in **2** is 2.365(3) Å, which is similar to the U–C distances for the alkyl group in an apical position in neutral **1** (2.368(7) and 2.380(7) Å), suggesting that the influence of increased uranium electrophilicity on the U–C_{alkyl} distance in **2** is partially offset by tighter XA_2 coordination combined with increased steric hindrance arising from η^6-arene coordination. The latter steric effect is supported by a more acute O–U–C_{apical} angle of 87.22(9)° in **2** (*cf.* 94.8(2) and 95.0(2)° in **1**). Compound **2** also exhibits an expanded U–C–Si angle of 133.8(2)° (*cf.* 128.2(3)-130.8(3)° in **1**), likely resulting from increased steric hindrance (or strengthened α-agostic interactions, although this seems less likely given that the U–C_{alkyl}–H angles in **2** {100(2)-102(2)°} are not especially acute[43]).

To the best of our knowledge, other structurally-characterized uranium alkyl cations are limited to compounds **a**,[44] **b** [45] and **c** [45] in Fig. 3, all of which feature anion or donor-solvent coordination.[47] The terminal U–C_{alkyl} bond length in **2** is very similar to those in methyl complexes **a** and **b** {2.39(1) and 2.395(6) Å, respectively}. By contrast, the U–C_{alkyl} distance in **c** is significantly longer than that in **2** as a result of polyhapto benzyl ligand coordination.

The U–C_{arene} distances in **2** range from 3.097(3) to 3.249(3) Å, resulting in a U–centroid distance of 2.86 Å and an average U–C_{arene} distance of 3.17 Å. Other structurally characterized uranium(IV) complexes featuring intermolecular coordination of a neutral arene are limited to Cotton's hexamethylbenzene species; dimetallic $[\{(\eta^6\text{-}C_6Me_6)UCl_2\}_2(\mu\text{-}Cl)_3][AlCl_4]$, and trimetallic $[\{(\eta^6\text{-}C_6Me_6)UCl_2(\mu\text{-}Cl)_3\}_2(UCl_2)]$, with average U–$C_{arene}$ distances of 2.92–2.94 Å, and average U–centroid distances of 2.55–2.58 Å.[48,49] The U–C_{arene} distances in Cotton's complexes are significantly shorter than those in **2**, presumably as a consequence of the increased donor ability of mesitylene *versus* benzene, decreased steric hindrance, and perhaps also increased electrophilicity at uranium.

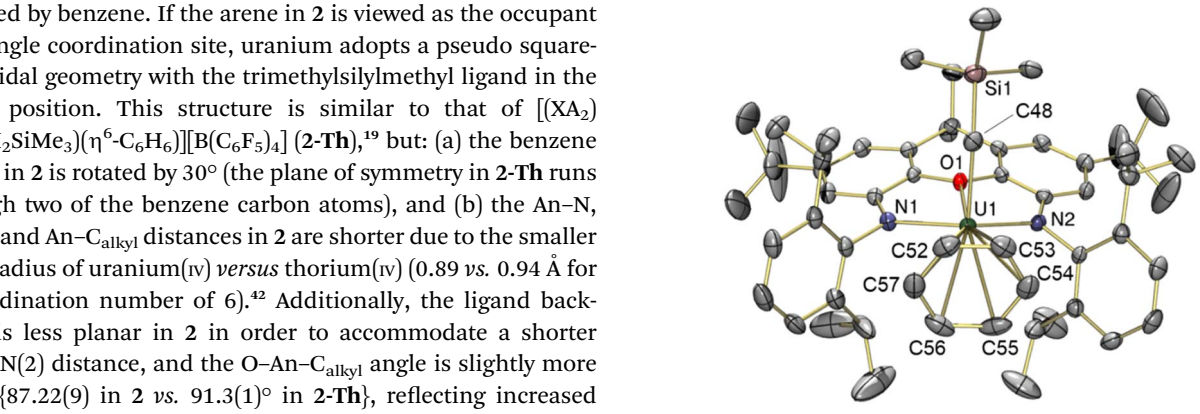

Fig. 2 X-ray crystal structure of $[(XA_2)U(CH_2SiMe_3)(\eta^6\text{-}C_6H_6)][B(C_6F_5)_4]\cdot 2$ benzene (**2**·2 benzene), with thermal ellipsoids at 50% probability. Hydrogen atoms, the borate anion, and two non-coordinated benzene solvent molecules are omitted for clarity. Selected bond distances (Å) and angles (°): U(1)–O(1) 2.440(2), U(1)–N(1) 2.236(2), U(1)–N(2) 2.223(2), U(1)–C(48) 2.365(3), U(1)–C(52) 3.249(3), U(1)–C(53) 3.187(3), U(1)–C(54) 3.108(3), U(1)–C(55) 3.097(3), U(1)–C(56) 3.159(3), U(1)–C(57) 3.243(3), U(1)–C_{arene} ave. 3.17, U(1)–Centroid 2.86, U(1)–C(48)–Si(1) 133.8(2), O(1)–U(1)–C(48) 87.22(9), N(1)–U(1)–N(2) 124.29(8).

The solid-state structure of toluene-coordinated **3** (Fig. 4) is similar to that of **2**, except that coordinated toluene is rotated approximately 30° relative to coordinated benzene in **2**, so that the C_{ipso}–C_{methyl} bond of toluene lies approximately in the plane of symmetry for the molecule, minimizing unfavourable steric interactions with the flanking 2,6-diisopropylphenyl groups. Furthermore, toluene in **3** is much less symmetrically bound than benzene in **2**, as demonstrated by the relatively shorter U–C_{para} (3.05(2) Å) and U–C_{meta} (3.13(2) and 3.36(2) Å) bonds, and relatively longer U–C_{ortho} (3.47(2) and 3.70(2) Å) and U–C_{ipso} (3.78(2) Å) distances, leading to an expanded U–centroid distance of 3.14 Å, and an average U–C_{arene} distance of 3.42 Å. All of these U–C_{arene} distances are above the sum of the covalent radii for U and C_{sp^2} (2.69 Å),[50] but are well within the sum of the van der Waals radii (4.48 Å).[51] However, an η^3-coordination mode is tentatively assigned, given that the O–U vector passes through toluene in much closer proximity to the *meta* and *para* carbon atoms; by comparison, the O–U vector in **2** approximately intersects with the centroid of benzene.

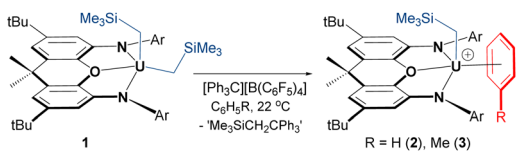

Scheme 1 Synthesis of monoalkyl uranium(IV) cations **2** and **3** (Ar = 2,6-diisopropylphenyl).

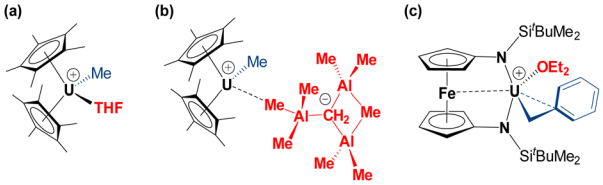

Fig. 3 Literature examples of crystallographically characterized uranium alkyl cations.[44–46]

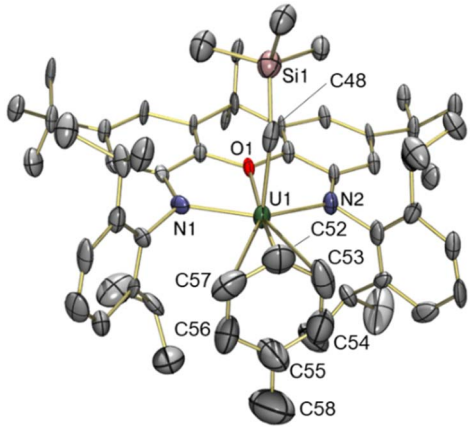

Fig. 4 X-ray crystal structure of $[(XA_2)U(CH_2SiMe_3)(\eta^3\text{-}C_6H_5Me)][B(C_6F_5)_4]\cdot$toluene (**3**·toluene), with thermal ellipsoids at 50% probability. Hydrogen atoms, the borate anion and a non-coordinated toluene solvent molecule are omitted for clarity. Selected bond distances (Å) and angles (°): U(1)–O(1) 2.417(9), U(1)–N(1) 2.22(1), U(1)–N(2) 2.21(1), U(1)–C(48) 2.36(2), U(1)–C(52) 3.05(2), U(1)–C(53) 3.13(2), U(1)–C(54) 3.47(2), U(1)–C(55) 3.78(2), U(1)–C(56) 3.70(2), U(1)–C(57) 3.36(2), U(1)–C_{arene} ave. 3.42, U(1)–Centroid 3.14, C(55)–C(58) 1.46(3), U(1)–C(48)–Si(1) 136.8(7), O(1)–U(1)–C(48) 88.8(4), N(1)–U(1)–N(2) 128.0(4).

The U–N {2.21(1) and 2.22(1) Å}, U–O {2.417(9) Å} and U–C_{alkyl} {2.36(2) Å} bond lengths, and the U–C_{alkyl}–Si {136.8(7)°} and O–U–C_{alkyl} {88.8(4)°} angles in **3** are very similar to those in **2**, suggesting that although toluene is an intrinsically superior donor, the steric inability of the bulkier arene to achieve an η^6-coordination mode limits the electron density it can provide to the metal centre, resulting in a similarly electrophilic cation. However, in contrast to the bent xanthene backbone (18.9°) of cation **2**, the ligand backbone in **3** is close to planar, with only a 5.9° angle between the xanthene aryl rings. This increase in backbone planarity is likely required to reposition the flanking isopropyl groups to sterically accommodate the methyl substituent of the toluene ligand; the shortest $Me_2HC\cdots CHMe_2$ distance (between the flanking 2,6-diisopropylphenyl groups) in **3** is 5.25 Å *versus* 4.54 Å in **2**.

Other toluene-coordinated uranium(IV) complexes have not been reported. However, we previously reported the toluene-coordinated thorium(IV) complex, $[(XA_2)Th(CH_2Ph)(\eta^6\text{-}C_6H_5Me)][B(C_6F_5)_4]$ (**e** in Fig. 1), which features a benzyl group in place of a (trimethylsilyl)methyl group. In this thorium benzyl cation, the arene occupies an axial rather than an equatorial position, and the Th–$C_{toluene}$ distances {3.063(5) to 3.435(6) Å} span a narrower range than those in **3**, leading to a substantially shorter An–centroid distance of 2.94 Å.[19]

In crystalline form, **2**·2 benzene and **3**·*x* toluene ($x = 1$ or 2) suffer from poor solubility in benzene or toluene,§ and as such, ^{1}H NMR spectra were recorded in bromobenzene-d_5, in which both cations dissolve readily. Upon dissolution of **2**·2 benzene and **3**·2 toluene in C_6D_5Br, the major signals in the room-temperature ^{1}H NMR spectra are identical, consisting of sixteen paramagnetically shifted and broadened signals ranging from +80 to −41 ppm. These resonances are consistent with an XA_2 uranium(IV) monoalkyl fragment with the expected C_s symmetry in solution. However, the presence of approximately three equivalents of free protio-benzene (from **2**·2 benzene) or protio-toluene (from **3**·2 toluene) indicates that the uranium-bound arenes of cations **2** and **3** are largely liberated upon dissolution in C_6D_5Br, generating $[(XA_2)U(CH_2SiMe_3)(C_6D_5Br)][B(C_6F_5)_4]$ (**4-*d*$_5$**; Scheme 2) *in situ* as the major product, in which bromobenzene may be π- or κ^1*Br*-coordinated. Cation **4-*d*$_5$** is also formed directly *via* the reaction of **1** with $[Ph_3C][B(C_6F_5)_4]$ in C_6D_5Br, with ^{2}H NMR resonances between −29 and −30 ppm for coordinated bromobenzene-d_5 (Fig. 5).

In order to observe the ^{1}H NMR signals for the XA_2 ligand and the alkyl group in **2** and **3**, samples of **2**·2 benzene and **3**·2 toluene were dissolved in C_6D_5Br spiked with 100 equivalents of C_6D_6 or $C_6D_5CD_3$, respectively. In each case, this yielded 16 resonances (these resonances were already present in low concentration when **2**·2 benzene or **3**·2 toluene was dissolved in neat C_6D_5Br) that are slightly shifted relative to those for **4-*d*$_5$**, indicating that the equilibrium has been driven almost entirely towards $[(XA_2)U(CH_2SiMe_3)(\eta^n\text{-}C_6D_5R)][B(C_6F_5)_4]$ (R = D (**2-*d*$_6$**) or CD_3 (**3-*d*$_8$**). As such, the binding preferences of the $[(XA_2)U(CH_2SiMe_3)]^+$ cation can be deduced to follow the order: toluene ≈ benzene > bromobenzene.

Upon dissolution of **2**·2 benzene in C_6D_5Br, the ^{1}H NMR signal for coordinated benzene in **2** (present in an approximate 1 : 5 ratio with **4-*d*$_5$**) was located at −29.4 ppm. This assignment was validated by independently synthesizing and isolating the deuterobenzene-coordinated cation, **2-*d*$_6$**·2 C_6D_6, which gave rise to a lone ^{2}H NMR resonance at −29.8 ppm in a C_6H_5Br solution spiked with 5 additional equivalents of C_6D_6 (Fig. 5). Furthermore, this ^{2}H NMR signal was completely eliminated upon subsequent addition of 100 equiv. of protio-benzene. Analogously, the ^{2}H NMR spectrum of **3-*d*$_8$**·2 C_7D_8 (in C_6H_5Br spiked with 5 equiv. of toluene-d_8) afforded four deuterium resonances at −17.5, −19.3, −22.8, and −67.3 ppm with relative integrations of 2 : 3 : 2 : 1, respectively (Fig. 5). These signals correlate to four low-intensity resonances in the ^{1}H NMR spectrum of **3**·2 C_7H_8 in pure C_6D_5Br, and were eliminated upon addition of 100 equivalents of protio-toluene.

Observation of signals for both free and coordinated benzene or toluene in the ^{1}H NMR spectra of **2**·2 benzene and **3**·2 toluene (in C_6D_5Br, with or without added benzene or toluene) demonstrates that degenerate exchange between free and coordinated arenes is slow on the NMR timescale at room temperature. This behaviour mirrors that previously reported for $[(XA_2)Th(CH_2SiMe_3)(\eta^6\text{-}C_6H_5Me)][B(C_6F_5)_4]$ (**3-Th**), for which

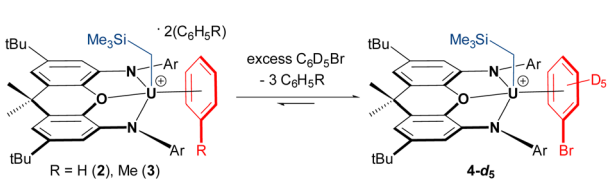

Scheme 2 *In situ* generation of C_6D_5Br-coordinated cation **4-*d*$_5$** (Ar = 2,6-diisopropylphenyl); although bromobenzene is depicted as π-coordinated, κ^1-coordination *via* bromine cannot be ruled out.

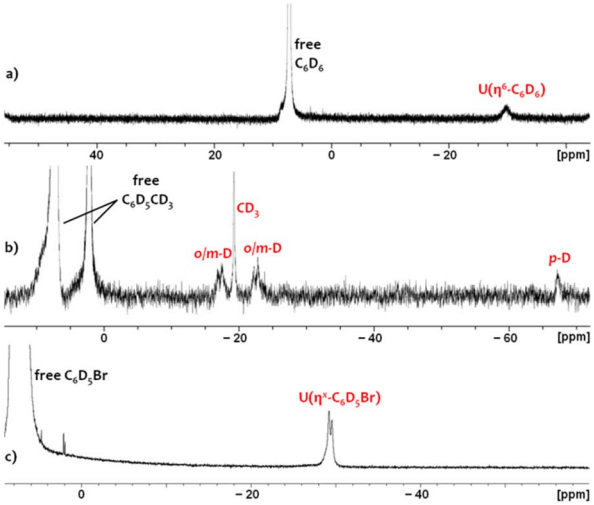

Fig. 5 ^{2}H NMR spectra of (a) **2-d_6** in C_6H_5Br containing 5 equiv. of C_6D_6, (b) **3-d_8** in C_6H_5Br containing 5 equiv. of toluene-d_8, and (c) **4-d_5** in neat C_6D_5Br.

well-separated ^{1}H and ^{13}C NMR resonances were observed for free and coordinated toluene at room temperature, with corresponding exchange cross peaks in the 2D-EXSY NMR spectrum. However, for **3-Th** in C_6D_5Br at the same concentration, no signals due to a bromobenzene-coordinated cation were observed, indicating that the equilibrium between a toluene- and a bromobenzene-coordinated cation lies substantially further towards the former in the case of thorium *versus* uranium.

In bromobenzene-d_5 solutions of **2**·2 benzene and **3**·2 toluene, the dominant cationic species, C_6D_5Br-bound **4-d_5**, is thermally stable for months at room temperature, and can tolerate heating at 60 °C for at least one hour with minimal decomposition. However, at 80 °C, **4-d_5** decomposed over the course of 8 hours, yielding a mixture of unidentified paramagnetic products and $SiMe_4$ as a major by-product. The thermal stability profile of cation **4-d_5** is very similar to that of its neutral dialkyl precursor **1**, which decomposes at 80 °C over the course of 24 hours. The stability of **4-d_5** is remarkable, given that cationic monoalkyl derivatives typically suffer from deteriorated thermal stability relative to their neutral dialkyl precursors. The high thermal stability of **4-d_5** in solution likely stems from the inflexibly positioned steric bulk of the XA_2 ligand combined with increased coordinative saturation afforded by bromobenzene coordination (most likely π-coordination given the similarity of the ^{1}H NMR spectra for **2-d_6**, **3-d_8** and **4-d_5**, and the observation of fluorobenzene π-coordination in **5**; *vide infra*). The effect of arene-coordination on thermal stability is also illustrated by the enhanced thermal stability of **3-d_8** generated in toluene-d_8;§ this cation is stable for at least 72 hours at 80 °C, only decomposing over 4 hours at 125 °C.

Neutral **1** and the thorium analogue **1-Th** are inactive for ethylene (1 atm) polymerization at 20, 70 and 100 °C in *n*-alkane solvents. Additionally, cationic **2–4** (in benzene, toluene, and bromobenzene, respectively), and the *in situ* generated thorium analogues of **2** and **3**, failed to yield polymer under 1 atm of ethylene at 20 and 70 °C. This suggests that, in these cations, ethylene is unable to compete with arene solvent for actinide coordination.

In an effort to implant the cationic $[(XA_2)U(CH_2SiMe_3)]^+$ fragment into a less coordinatively supportive environment, the reaction of **1** with $[Ph_3C][B(C_6F_5)_4]$ was conducted in fluorobenzene, resulting in a change in the solution colour from bright-red to deep-brown. Crystals of $[(XA_2)U(CH_2SiMe_3)(\eta^3\text{-}C_6H_5F)][B(C_6F_5)_4]\cdot C_6H_5F$ (**5**·C_6H_5F; *vide infra*) were isolated after crystallization from C_6H_5F/*n*-pentane at −30 °C, and **5** (free from non-coordinated fluorobenzene) was obtained in 91% yield after exposure to vacuum (Scheme 3).

In C_6D_5Br, cation **5** is converted entirely to bromobenzene-bound **4-d_5**, with release of one equivalent of free fluorobenzene. Therefore, fluorobenzene-coordinated **5** was generated directly in C_6H_5F spiked with approximately 10% cyclohexane-d_{12}. At room temperature, the ^{1}H NMR spectrum of **5** in C_6H_5F/C_6D_{12} revealed only six resonances; those for the *tert*-butyl groups, the *para*-positions of the 2,6-diisopropylphenyl rings, the $CH^{1,8}$ and $CH^{3,6}$ positions of the xanthene backbone, and the UCH_2 and $SiMe_3$ protons. All XA_2 protons located above/below the plane of the xanthene backbone of the XA_2 ligand were broadened to the extent that they were not observed. These data are indicative of rapid migration of the CH_2SiMe_3 group from one side of the ligand backbone to the other, which requires dissociation and re-association of coordinated fluorobenzene (or degenerate associative substitution); Scheme 3. However, at −36 °C, 16 signals ranging from +107 to −91 ppm were observed, consistent with a C_s-symmetric cation, as observed for **2–4** at 25 °C (^{1}H or ^{19}F NMR signals for coordinated C_6H_5F could not be located).

The solid state structure of **5** revealed a familiar arene solvent-separated ion pair with approximate C_s-symmetry, comprised of a uranium(IV) cation with an axially-positioned trimethylsilyl-methyl ligand, and fluorobenzene π-coordinated in the plane of the ligand (Fig. 6). The C_{ipso}–F bond length in **5** {1.362(7) Å} is significantly shorter than the C_{ipso}–C_{methyl} distance in **3** {1.47(3) Å}, and is equal within error to that for free

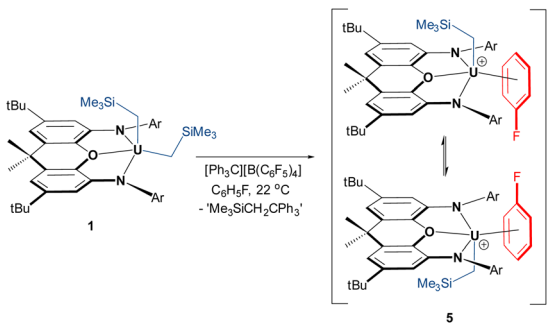

Scheme 3 Synthesis of fluorobenzene-coordinated uranium alkyl cation **5** (Ar = 2,6-diisopropylphenyl), which in solution, on the NMR timescale, undergoes rapid migration of the alkyl group from one side of the plane of the ligand backbone to the other.

fluorobenzene {1.355(2) Å from gas phase electron diffraction}.[52]

Structurally, **5** bears resemblance to **3**, with very similar U–N and U–C_{alkyl} bond distances, a relatively planar xanthene backbone (the angle between the xanthene aryl rings is 7.1°), and an arene ligand that is asymmetrically coordinated as a consequence of monosubstitution. The C–F bond of the fluorobenzene ligand lies approximately in the plane of symmetry of the molecule. However, the fluorine substituent of fluorobenzene is significantly smaller[53,54] than the methyl group of toluene, resulting in shorter U–C_{ipso} and longer U–C_{para} distances in **5**, and a shorter U–centroid distance (3.08 Å in **5** *vs.* 3.14 Å in **3**).

Compound **5** is the first crystallographically-characterized example of an f-element bound to a neutral fluoroarene. The majority of complexes bearing π-coordinated fluoroarene ligands contain electron-rich transition metals with d^6, d^8 and d^{10} electronic configurations.[55] By contrast, fluoroarenes coordinated to electrophilic early transition metal centres tend to be κ^1-*F* coordinated (Fig. 7).[56–58]

A 1 mM solution of $[(XA_2)U(CH_2SiMe_3)(\eta^3\text{-}C_6H_5F)][B(C_6F_5)_4]$ (**5**) in fluorobenzene under ethylene (1 atm; 20 °C; 30 min) achieved a polymerization activity of 52 400 g mol^{-1} h^{-1} atm^{-1}; a stark contrast to the lack of polymerization observed for cations generated in benzene, toluene and bromobenzene. This confirms that XA_2 uranium(IV) alkyl complexes can in fact serve as ethylene polymerization catalysts in the absence of competitively binding arene solvents, and the activity of **5** increased slightly to 60 000 g mol^{-1} h^{-1} atm^{-1} at 70 °C (Table 1). The relatively small increase in activity from 20 to 70 °C suggests that catalyst deactivation becomes significant at higher temperature, and indeed, reducing the polymerization time (at 70 °C) to 5 minutes afforded an activity of 139 200 g mol^{-1} h^{-1} atm^{-1}.

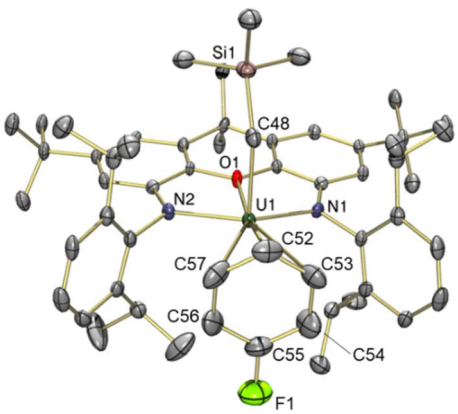

Fig. 6 X-ray crystal structure of $[(XA_2)U(CH_2SiMe_3)(\eta^3\text{-}C_6H_5F)][B(C_6F_5)_4]\cdot$fluorobenzene (**5**·fluorobenzene), with thermal ellipsoids at 50% probability. Hydrogen atoms, the borate anion, and non-coordinated fluorobenzene lattice solvent are omitted for clarity. Selected bond distances (Å) and angles (°): U(1)–O(1) 2.431(3), U(1)–N(1) 2.215(3), U(1)–N(2) 2.217(3), U(1)–C(48) 2.351(4), U(1)–C(52) 3.126(5), U(1)–C(53) 3.296(5), U(1)–C(54) 3.527(5), U(1)–C(55) 3.594(5), U(1)–C(56) 3.434(5), U(1)–C(57) 3.215(6), U(1)–F(1) 4.528(4), U(1)–C_{arene} ave. 3.37, U(1)–Centroid 3.08, C(55)–F(1) 1.362(7), U(1)–C(48)–Si(1) 134.9(2), O(1)–U(1)–C(48) 89.4(1), N(1)–U(1)–N(2) 127.6(1).

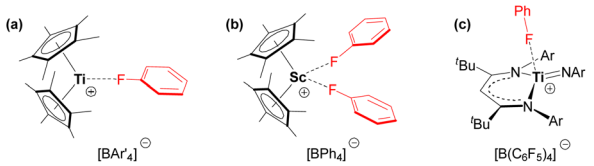

Fig. 7 Fluoroarene complexes of electrophilic transition metals. (a) $[(Cp^*)_2Ti(\kappa^1\text{-}FC_6H_5)][BAr'_4]$ (Ar′ = Ph or C_6F_5), (b) $[(Cp^*)_2Sc(\kappa^1\text{-}FC_6H_5)_2][BPh_4]$, and (c) [(nacnac)Ti=NAr(κ^1-FC_6H_5)][$B(C_6F_5)_4$] (nacnac = $\{CH(C(^tBu)NAr)_2\}^-$; Ar = 2,6-diisopropylphenyl).[56–58]

Based on the success of **5** as a polymerization catalyst in fluorobenzene, the reaction of colourless **1-Th** with one equiv. of $[Ph_3C][B(C_6F_5)_4]$ was also carried out in fluorobenzene, forming a vibrant orange solution over the course of 3.5 hours, which polymerized ethylene (1 atm) with an activity of 16 800 g mol^{-1} h^{-1} atm^{-1} at 20 °C (the same activity was obtained after activation for 24 hours), and 57 600 g mol^{-1} h^{-1} atm^{-1} at 70 °C, illustrative of appreciable thorium catalyst thermal stability. To the best of our knowledge, cationic **5** and **5-Th** are the most active non-cyclopentadienyl actinide catalysts for homogeneous ethylene polymerization reported to date.

Reaction of **1** with $[Ph_3C][B(C_6F_5)_4]$ in 1,2-difluorobenzene also yielded a deep brown solution, providing ethylene polymerization activities of 11 200 and 0 g mol^{-1} h^{-1} atm^{-1} at 20 and 70 °C, respectively (Table 1), indicating that the catalytic species formed in 1,2-difluorobenzene is less thermally stable than that formed in fluorobenzene; the ^{1}H NMR spectrum of the

Table 1 Ethylene polymerization activities for $[(XA_2)An(CH_2SiMe_3)(arene)_n][B(C_6F_5)_4]$ (An = U or Th; n = 1 or 0) under 1 atm of ethylene.[a,b]

M	Solvent	Temp (°C)	PE (g)	Activity[c]	T_m[d] (°C)
U, Th	C_6H_6	20, 70	0	0	n/a
U, Th	C_6H_5Me	20	0	0	n/a
U, Th	alkane[e]	20, 70	0	0	n/a
U	C_6H_5Br	20, 70	0	0	n/a
U	C_6H_5F	20	0.131	52 400	130.6
U	C_6H_5F	70	0.150	60 000	127.0
U	C_6H_5F[f]	70	0.058	139 200	126.5
Th	C_6H_5F	20	0.042	16 800	136.7
Th	C_6H_5F	70	0.144	57 600	131.6
U	*o*-$C_6H_4F_2$	20	0.028	11 200	125.9
U	*o*-$C_6H_4F_2$	70	0	0	n/a

[a] Polymerization conditions: 0.005 mmol of catalyst (<10 mg), 5 mL of solvent, 30 min (arene solvents; unless otherwise specified) or 24 hours (alkane solvents). [b] Catalysts were generated *in situ* by reaction of $[(XA_2)An(CH_2SiMe_3)_2]$ with $[CPh_3][B(C_6F_5)_4]$; these reactions were allowed to proceed for 30 minutes (in C_6H_6, C_6H_5Me, C_6H_5Br, or *o*-$C_6H_4F_2$), 3.5 hours (in C_6H_5F), or 24 hours {in alkane solvents under ethylene (1 atm)}. [c] Activities are measured in (g of PE)·(mol of An)$^{-1}$·h^{-1}·(atm of C_2H_4)$^{-1}$. [d] Peak melting temperature, T_m, from DSC (re-melt). [e] Reactions were carried out in alkane with (i) 0 equiv. of added arene solvent (Th and U), (ii) 3 equiv. of added toluene (U only), and (iii) 3 equiv. of added C_6H_5F (U only). For polymerization reactions at 20 °C, alkane = hexanes. For polymerization reactions at 70 °C, alkane = *n*-heptane. [f] A shorter polymerization time of 5 minutes was used.

cation generated in 9 : 1 *o*-$C_6H_4F_2/C_6D_{12}$ at 20 °C was not clean and was accompanied by significant $SiMe_4$ evolution, suggestive of competitive cation formation and decomposition. Furthermore, reactions between **1** or **1-Th** and $[Ph_3C][B(C_6F_5)_4]$ in alkane solvents (generated over 24 hours under 1 atm of ethylene at 20 °C; for uranium, with or without 3 equiv. of added toluene or fluorobenzene) did not yield an active polymerization catalyst; with **1**, cation decomposition afforded a grey precipitate and considerable amounts of $H_2(XA_2)$. A similar lack of polymerization activity was observed for cations generated from **1** in 1,3-difluorobenzene, mesitylene, C_6F_6, and α,α,α-trifluorotoluene,¶ indicating that C_6H_5F achieves a delicate balance between being sufficiently coordinating to stabilize the required alkyl cation, and sufficiently labile to allow ethylene to access the metal centre. The choice of alkyl group also plays an important role in determining catalytic activity, given that the reaction of the dibenzyl complex, $[(XA_2)U(CH_2Ph)_2]$ (**6**; prepared from the reaction of $[(XA_2)UCl_3K(dme)_3]$ with 2 equiv. of KCH_2Ph; an X-ray crystal structure is provided in Fig. S20‡), with $[Ph_3C][B(C_6F_5)_4]$ in fluorobenzene¶ failed to yield an active polymerization catalyst under ethylene (1 atm) at 20 or 70 °C.

Polyethylene produced using fluorobenzene-bound **5** and the thorium analogue, **5-Th**, was insufficiently soluble in 1,2,4-trichlorobenzene at 140 °C for analysis by Gel Permeation Chromatography (GPC). The limited solubility of these polymers suggests that they are of high molecular weight, which is supported by the high peak melting temperatures (T_m; from Differential Scanning Calorimetry (DSC) re-melt) which range from 125.9 to 136.7 °C.[59] However, polyethylene formed using the unstable catalyst generated in 1,2-difluorobenzene could be solubilised, and GPC analysis indicates a polymer of moderate molecular weight, with an M_w of 2.9×10^4 and M_n of 1.1×10^4 g mol^{-1}, and a polydispersity index (PDI) of 2.61, which is sufficiently low, considering the low thermal stability of the catalyst, to suggest a single-site polymerization mechanism.[39]

Computational studies

To gain insight into the nature and relative strength of actinide–arene bonding in **2**, **2-Th**, **3**, and **5**, we turned to DFT calculations (ADF/AMS, gas-phase, all-electron (without frozen cores), PBE, D3-BJ, TZ2P, scalar ZORA, charge +1, C_S symmetry; for uranium complexes, spin-unrestricted with a spin polarization of 2). Calculations were carried out on the cationic portion of analogues of **2**, **3**, and **5** in which the two methyl groups and two *tert*-butyl groups on the xanthene backbone were replaced by hydrogen atoms: $[(XA_{2'})U(CH_2SiMe_3)(arene)]^+$ {arene = benzene (**2′**), toluene (**3′**) and fluorobenzene (**5′**)}. The geometry optimized structures of **2′**, **3′**, and **5′** match well with the X-ray crystal structures of **2**, **3** and **5**; the U–N, U–O, and U–C_{alkyl}, bonds are within 0.03–0.06 Å of the crystallographic values, which is within the expected accuracy of the method, and the U–C–Si and O–U–$arene_{centroid}$ angles are reproduced to within 4°. The U–$arene_{centroid}$ distances in **2′**, **3′** and **5′** are slightly overestimated, with calculated values that are 0.04, 0.19 and 0.10 Å longer than the experimental values for **2**, **3** and **5**. For **3′** and **5′**, this is concomitant with an overestimation of the U–$arene_{centroid}$–C_{ipso} angles, although the greater deviation in the case of **3′** may be due to the lower quality X-ray structure of **3**.

For $[(XA_{2'})U(CH_2SiMe_3)(C_6H_5F)]^+$, a slightly higher energy minimum (**5a′**) in which fluorobenzene is η^4-coordinated *via* the *ipso* and *ortho* carbon atoms as well as fluorine was also located. Attempted geometry optimization starting from a structure in which one molecule of fluorobenzene is κ^1F-coordinated lead only to **5′** or **5a′**, although a minimum with two κ^1F-coordinated fluorobenzene ligands (**5b′**) was located (without symmetry constraints). Values of ΔG (298 K) for conversion of **5′** to **5a′** or **5b′** were 3.3 and 15.0 kJ mol^{-1}, respectively, suggesting that **5a** and **5b** may play a role in fluorobenzene solutions of **5**. Computational analysis of the bonding in **5a′** and **5b′** is provided in the ESI.‡

Spin-restricted calculations were also carried out on $[(XA_{2'})Th(CH_2SiMe_3)(\eta^6\text{-benzene})]^+$ (**2′-Th**), and C_s symmetric structures which differ from one another by a 30° rotation in the benzene ligand (around the Th–$benzene_{centroid}$ axis) were found to lie within 1 kJ mol^{-1} of one another: the structure in which the plane of symmetry runs through two of the benzene carbon atoms was used for further discussion since this orientation matches that in the solid state structure. The Th–N, Th–O, Th–C_{alkyl}, and Th–$arene_{centroid}$ distances are within 0.01–0.06 Å of the crystallographic values for **2-Th**,[19] and the Th–C–Si and O–Th–$arene_{centroid}$ angles are reproduced to within 0.2° and 10° respectively (this structure is only 3.5 kJ mol^{-1} lower in energy than the structure constrained to have the same O–Th–$arene_{centroid}$ angle as the X-ray crystal structure).

Significant An–C Mayer bond orders[60] were observed to all six benzene carbon atoms in **2′** (0.12–0.14) and **2′-Th** (0.08–0.09), reflective of η^6-arene coordination; for comparison, the An–C_{alkyl} bonds in **2′** and **2′-Th** have Mayer bond orders of 0.72 and 0.66, respectively. By contrast, approximate η^3-toluene and η^3-fluorobenzene coordination in **3′** and **5′** results in significant (>0.10) Mayer bond orders between uranium and the *meta* and *para* arene carbon atoms (0.17 and 0.14 to the *para* carbon, and 0.10 and 0.11 to the *meta* carbon atoms, respectively), whereas the U–C Mayer bond orders to the *ipso* and *ortho* arene carbon atoms are 0.05 or less.

Actinide–arene bonding was further investigated by considering the interactions between the $(XA_{2'})An(CH_2SiMe_3)^+$ and arene fragments in **2′-Th**, **2′**, **3′** and **5′** using the energy decomposition analysis[61] of Ziegler and Rauk.[62,63] This approach affords an overall interaction energy, ΔE_{int}, which is divided into five components:

$$\Delta E_{int} = \Delta E_{elec} + \Delta E_{orb} + \Delta E_{disp} + \Delta E_{Pauli} + \Delta E_{prep} \quad (1)$$

The ΔE_{elec} component represents the electrostatic interaction energy (calculated using frozen charge distributions for both fragments), ΔE_{orb} is the orbital interaction energy (this term includes all contributions resulting from intrafragment polarization), ΔE_{disp} is the dispersion interaction energy, ΔE_{Pauli} corresponds to Pauli repulsion, and ΔE_{prep} is the energy needed to bring the fragments from their optimum geometries to their geometries in the unfragmented complex.

Table 2 Data from fragment interaction calculations ($[(XA_{2'})An(CH_2SiMe_3)]^+$ + arene) on **2′-Th**, **2′**, **3′** and **5′**. All energies are in kJ mol^{-1}, ΔE_{int} values are BSSE-corrected, and for ETS-NOCV data, values in parentheses are percentages of ΔE_{orb}. See text for a description of the ETS-NOCV contributions ΔE_1–ΔE_5

		2′-Th	**2′**	**3′**	**5′**
	Arene	C_6H_6	C_6H_6	C_6H_5Me	C_6H_5F
EDA	ΔE_{elec}	−112.2	−139.9	−119.4	−109.7
	ΔE_{orb}	−123.8	−141.6	−111.5	−110.0
	ΔE_{Pauli}	160.1	213.7	165.9	164.5
	ΔE_{Disp}	−63.2	−63.2	−60.7	−59.9
	ΔE_{prep}	28.4	32.6	28.3	28.6
	BSSE	−6.8	−7.5	−7.0	−7.5
	ΔE_{int}	−104.0	−90.9	−90.4	−79.0
ETS-NOCV	ΔE_1	−30.7 (25%)	−32.0 (23%)	−35.9 (32%)	−29.4 (27%)
	ΔE_2	−24.7 (20%)	−23.4 (17%)	−14.1 (13%)	−15.2 (14%)
	ΔE_3	−25.2 (20%)	−24.6 (17%)	−7.3 (6%)	−11.7 (11%)
	ΔE_4	—	−8.2 (6%)	−10.2 (9%)	−9.0 (8%)
	ΔE_5	—	−9.4 (7%)	−8.4 (7%)	−10.0 (9%)
	Other	−44.0 (35%)	−44.4 (31%)	−36.2 (32%)	−35.3 (32%)

Energy decomposition analysis of **2′-Th**, **2′**, **3′** and **5′** afforded interaction energies (ΔE_{int}; BSSE-corrected) of −104, −91, −90 and −79 kJ mol^{-1}, respectively (Table 2), indicating that (a) benzene is more tightly coordinated in the thorium cation than the uranium cation, likely due to reduced steric hindrance around the larger metal (*vide infra*), and (b) the strength of uranium–arene bonding decreases in the order **2′** ≈ **3′** > **5′**. Weaker fluorobenzene binding is consistent with the results of solution NMR studies on **2**, **3** and **5**, and the high ethylene polymerization activity of **5** compared to **2** and **3**, which were catalytically inactive (*vide supra*).

In benzene-coordinated **2′**, the ΔE_{orb} (−142 kJ mol^{-1}) and ΔE_{elec} (−140 kJ mol^{-1}) contributions to bonding are nearly identical, indicative of substantial covalent character in the U–benzene interaction. Bonding between benzene and the $(XA_{2'})An(CH_2SiMe_3)^+$ fragment in **2′-Th** involves weaker orbital and electrostatic interactions than in the **2′** (by 18 and 28 kJ mol^{-1}, respectively), but a more negative ΔE_{int} is obtained due to significantly reduced Pauli repulsion around the larger actinide element (ΔE_{Pauli} is 54 kJ mol^{-1} lower in **2′-Th** than in **2′**).

While ΔE_{int} is very similar for U–toluene bonding in **3′** and U–benzene bonding in **2′**, significant differences are observed in the individual contributors: ΔE_{elec} and ΔE_{orb} in **3′** are less negative by 21 and 31 kJ mol^{-1} as a consequence of η^3-coordination, but this coordination mode also reduces ΔE_{Pauli} by 48 kJ mol^{-1}. Bonding between U(IV) and fluorobenzene in **5′** involves very similar ΔE_{orb} and ΔE_{Pauli} contributions to those in **3′** (within 1.5 kJ mol^{-1}), likely because the reduced donor ability of fluorobenzene is offset by closer approach of this less-hindered arene (the U–arene$_{centroid}$ distance is 3.18 Å in **5′** *versus* 3.33 Å in **3′**). However, U–C_6H_5F bonding is weaker overall due to a 9 kJ mol^{-1} reduction in ΔE_{elec} resulting from the electron withdrawing character of the fluorine substituent. Notably, the dispersion interactions between the metal fragment and each of the three arenes are nearly identical in energy (between −60 and −63 kJ mol^{-1}), as are the preparation energies for these structures (between 28 and 33 kJ mol^{-1}).

The deformation density ($\Delta\rho$) associated with the orbital interaction component (ΔE_{orb}) of the arene–metal interactions in **2′**, **2′-Th**, **3′**, and **5′** was further divided using the Extended Transition State and Natural Orbitals for Chemical Valence (ETS-NOCV) method[64–67] (Table 2; deformation density isosurfaces are shown in Fig. 8; the NOCVs and fragment orbitals associated with each of the ETS-NOCV contributions are shown in Fig. S29–S43‡). For **2′**, five distinct contributions were elucidated, labelled $\Delta\rho_1$–$\Delta\rho_5$ (with energies ΔE_1–ΔE_5).‖ These five interactions sum to 69% of ΔE_{orb}, with many smaller contributions accounting for the remaining 31%. $\Delta\rho_1$ and $\Delta\rho_2$ involve π-donation to uranium from the two highest-energy occupied π-molecular orbitals of benzene ($\Psi_{\pi2}$ and $\Psi_{\pi3}$), whereas $\Delta\rho_3$ involves σ-donation to uranium from the lowest energy benzene π-molecular orbital ($\Psi_{\pi1}$); the most significant fragment orbitals contributing to $\Delta\rho_1$, $\Delta\rho_2$ and $\Delta\rho_3$ (for **2′**) are depicted in Fig. 8. By contrast, $\Delta\rho_4$ and $\Delta\rho_5$ involve transfer of an unpaired electron between f-orbitals, due to changes in f-orbital energy upon arene coordination. The relative energies of these components are $\Delta E_1 > \Delta E_2 \approx \Delta E_3 > \Delta E_4 \approx \Delta E_5$. The metal acceptor orbitals associated with $\Delta\rho_1$, $\Delta\rho_2$ and $\Delta\rho_3$ have significant uranium 5f, 6d, 7s and/or 7p character; details are provided in Fig. S29–S43.‡ ETS-NOCV calculations on the thorium analogue, **2′-Th**, afforded very similar results, but without the $\Delta\rho_4$ and $\Delta\rho_5$ contributions due to an absence of f-electrons (Table 2).

ETS-NOCV calculations on toluene- and fluorobenzene-coordinated **3′** and **5′** afforded a similar set of five major contributions ($\Delta\rho_1$–$\Delta\rho_5$; Table 2 and Fig. 8), but with the following differences arising from approximate η^3-arene coordination: (a) whereas $\Delta\rho_1$ for **2′** involves π-donation from the benzene HOMO ($\Psi_{\pi3}$) to uranium, $\Delta\rho_1$ for **3′** and **5′** involves σ-donation; mixing of the $\Psi_{\pi1}$ and $\Psi_{\pi3}$ orbitals cancels the wavefunction on part of the aromatic ring and enhances it on the other, leading to bonding involving primarily the *meta* and *para* carbon atoms. The resulting ΔE_1 (−36 kJ mol^{-1} for **3′** and −29 kJ mol^{-1} for **5′**) is comparable to that for **2′** (−32 kJ mol^{-1}).

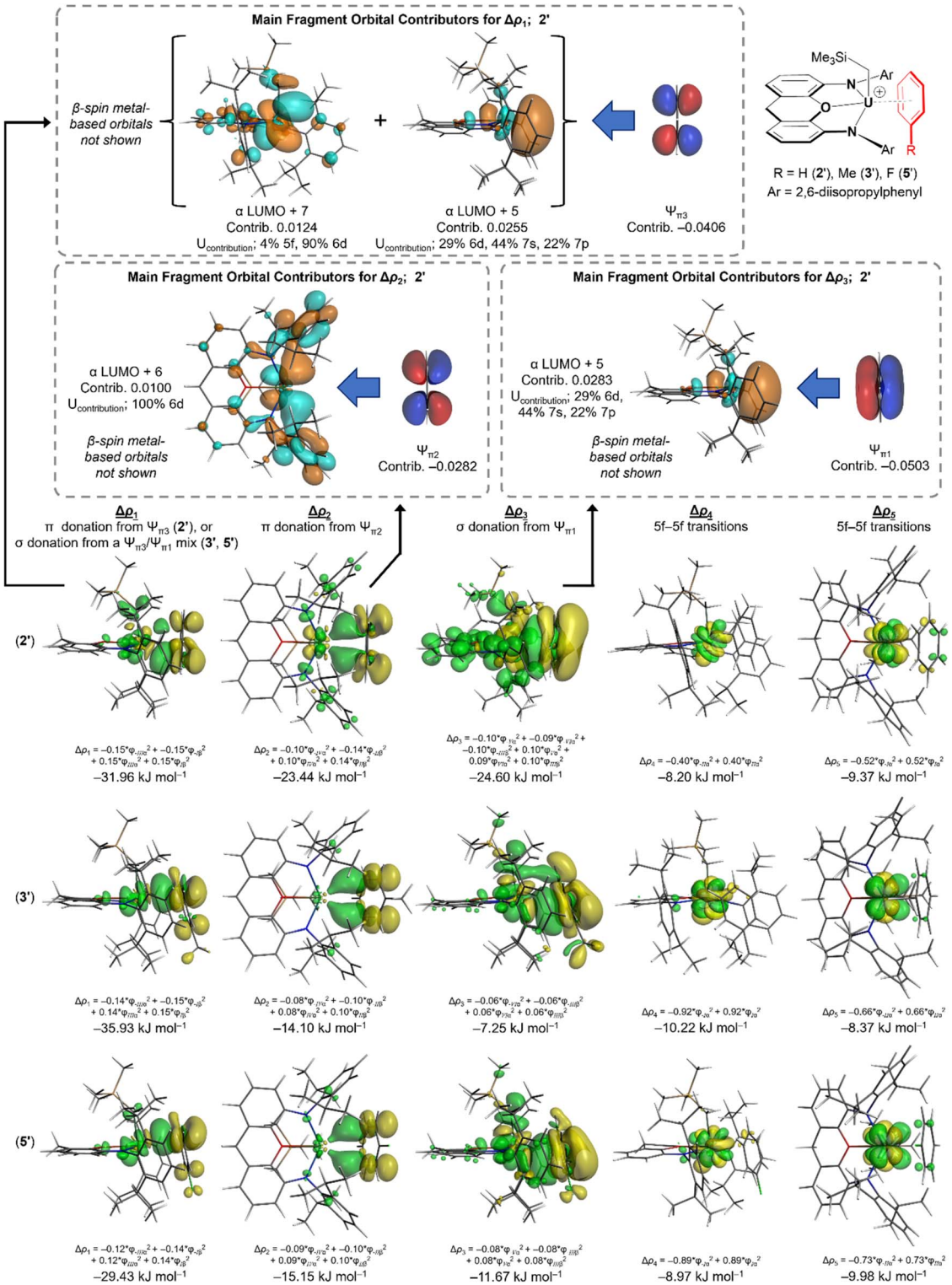

Fig. 8 Deformation density contributions $\Delta\rho_1$, $\Delta\rho_2$, $\Delta\rho_3$, $\Delta\rho_4$, and $\Delta\rho_5$ (each $\Delta\rho_n$ figure is the sum of the α and β contributions) to bonding between the $(XA_{2'})U(CH_2SiMe_3)^+$ and arene fragments in $[(XA_{2'})U(CH_2SiMe_3)(benzene)]^+$ (**2'**), $[(XA_{2'})U(CH_2SiMe_3)(toluene)]^+$ (**3'**), and $[(XA_{2'})U(CH_2SiMe_3)(fluorobenzene)]^+$ (**5'**). Increased (green) and decreased (yellow) electron density is presented relative to the fragments, and isosurfaces are set to 0.0003 ($\Delta\rho_1$ and $\Delta\rho_2$), 0.00005 ($\Delta\rho_3$), and 0.001 ($\Delta\rho_4$ and $\Delta\rho_5$). Dashed boxes at the top of the figure show the main α-spin fragment orbital contributors for $\Delta\rho_1$, $\Delta\rho_2$, and $\Delta\rho_3$ in **2'** (filled orbitals are shaded dark blue and red, whereas virtual orbitals are shaded in pale blue and orange; isosurfaces are set to 0.03). The character (% 5f, % 6d *etc.*) of uranium atomic orbitals contributing to $(XA_{2'})U(CH_2SiMe_3)^+$ fragment orbitals in **2'** is provided (only values ≥ 3% are included) – these values are normalized to the total of all uranium contributions (those contributing 1% or more to the total for the fragment orbital).

(b) The π-donor interaction associated with $\Delta\rho_2$ in **3′** and **5′** is less effective than that in **2′**, resulting in ΔE_2 values of −14 and −15 kJ mol^{-1} respectively (*cf.* −23 kJ mol^{-1} for **2′**). (c) The $\Delta\rho_3$ interaction (involving σ-donation from $\Psi_{\pi 1}$ to uranium) is significantly weaker in **3′** and **5′**, giving rise to ΔE_3 values of −7 and −12 kJ mol^{-1} respectively (*cf.* −25 kJ mol^{-1} for **2′**).

Summary and conclusions

A series of uranium cations, $[(XA_2)U(CH_2SiMe_3)(\eta^n\text{-arene})][B(C_6F_5)_4]$ {arene = benzene (**2**), toluene (**3**), bromobenzene (**4**) and fluorobenzene (**5**)} have been isolated (**2**, **3** and **5**) or generated *in situ* (**4**). ^{2}H NMR signals were observed for the coordinated arene in **2-*d*$_6$** in C_6H_5Br containing 2 or more equiv. of C_6D_6, **3-*d*$_8$** in C_6H_5Br containing 2 or more equiv. of toluene-d_8, and **4-*d*$_5$** in neat C_6D_5Br. By contrast, signals for coordinated C_6H_5F in **5** (in a 9 : 1 mixture of C_6H_5F/cyclohexane-d_{12}) could not be located, and fluxional room temperature behaviour (involving rapid migration of the uranium alkyl group from one side of the xanthene backbone to the other) is consistent with rapid fluorobenzene dissociation and re-association from **5** (or degenerate associative substitution). These data suggest that the binding preferences of the $[(XA_2)U(CH_2SiMe_3)]^+$ cation follow the order: toluene ≈ benzene > bromobenzene > fluorobenzene.

Compounds **2**·2 benzene, **3**·toluene, and **5**·fluorobenzene were crystallographically characterized, and are rare examples of arene-coordinated alkyl cations. Compound **5** is the first structurally-characterized example of an f-element complex bearing a neutral fluoroarene ligand, and π-coordination of fluorobenzene in **5** is unusual, given that fluorobenzene is κ^1-*F*-coordinated in all crystallographically characterized group 3 and 4 fluorobenzene complexes.

Cations **2–4**, and the thorium analogues (**2-Th** and **3-Th**)[19] are inactive for ethylene (1 atm) polymerization. By contrast, cations generated in fluorobenzene (**5** and the thorium analogue **5-Th**) achieved moderate to high activities,[68] highlighting the extent to which common arene solvents such as toluene can reduce or quench polymerization activity, especially for sterically-open post-metallocene f-element alkyl cations. Uranium alkyl cation generation in less-donating *o*-$C_6H_4F_2$ also afforded an active polymerization catalyst, but with diminished thermal stability. Furthermore, actinide cation generation in hexanes led to extensive decomposition, and did not give rise to an active catalyst system, and similar results were obtained for cations generated from **1** in arene solvents which are less-able to coordinate as a consequence of increased steric hindrance and/or reduced donor ability (*m*-$C_6H_4F_2$, C_6F_6, $C_6H_5CF_3$ and mesitylene). These results highlight the extent to which C_6H_5F achieves the right balance between being sufficiently coordinating to stabilize the uranium and thorium alkyl cations, and sufficiently labile to provide ethylene with access to the metal centre.

DFT calculations were carried out to gain insight into the nature of actinide–arene bonding in the cationic portion of **2**, **2-Th**, **3**, and **5**. Key findings were: (a) actinide–arene bonding in **2′**, **2′-Th**, **3′** and **5′** (analogues of **2**, **2-Th**, **3** and **5** with hydrogen atoms in place of ligand backbone methyl and *tert*-butyl groups) is appreciably covalent, with similar values of the orbital interaction and electrostatic contributions. (b) Benzene is more tightly coordinated in the thorium cation (**2′-Th**) than the uranium cation (**2′**). This is due to reduced steric hindrance around the larger metal, and occurs even though the orbital interaction and electrostatic contributions to bonding are diminished for **2′-Th** *versus* **2′**. (c) η^3-arene coordination reduces the orbital interaction and electrostatic contributions to bonding in toluene-coordinated **3′**, relative to **2′**, but a concomitant decrease in Pauli repulsion leads to a nearly identical overall interaction energy. (d) Bonding between U(IV) and fluorobenzene (in **5′**) affords orbital interaction and Pauli repulsion contributions that are similar to those in toluene-coordinated **3′**, likely because the reduced donor ability of fluorobenzene is offset by closer approach of the less sterically hindered arene. However, the overall interaction energy is ∼10 kJ mol^{-1} less negative due to a reduction in the electrostatic contribution to bonding (resulting from the electron withdrawing character of the fluorine substituent). (e) ETS-NOCV calculations indicate that bonding in **2′** involves σ- and π-donation (×2) from the three filled π-molecular orbitals of benzene, as well as transfer of the two unpaired electrons between f-orbitals (due to changes in f-orbital energy upon arene coordination). (f) ETS-NOCV calculations on **2′-Th** were very similar to those for **2′**, but without the intra-fragment f-electron transfer, due to an absence of f-electrons. (g) ETS-NOCV calculations on **3′** and **5′** afforded a related bonding picture, but with differences due to the η^3-arene coordination mode, resulting in weakening of two of the orbital interaction contributions. Overall, the strength of actinide–arene bonding decreased in the order **2′-Th** > **2′** ≈ **3′** > **5′**. Weaker fluorobenzene binding (in **5**) is consistent with the results of solution NMR studies on **2**, **3** and **5**, and the high ethylene polymerization activity of **5** compared to that of **2**, **2-Th**, and **3**, which were catalytically inactive.

Experimental section

General details

An argon-filled MBraun UNIlab glove box equipped with a −30 °C freezer was employed for the manipulation and storage of air-sensitive ligands and complexes. Preparative reactions were performed on a double manifold high vacuum line equipped with an Edwards RV12 vacuum pump (ultimate pressure 1.5 × 10^{-3} torr) using standard techniques,[69] and vacuum was measured periodically using a Varian Model 531 Thermocouple Gauge Tube with a Model 801 Controller. Residual oxygen and moisture was removed from the argon or ethylene stream by passage through an Oxisorb-W scrubber from Matheson gas products. Commonly utilized specialty glassware includes the swivel frit assembly, thick-walled Straus flasks equipped with Teflon stopcocks, and J-Young or Wilmad-LabGlass LPV NMR tubes. A VWR Clinical 200 Large capacity centriguge (with 28° fixed-angle rotors that hold 12 × 15 mL or 6 × 50 mL tubes, and in combination with VWR high-performance polypropylene conical centrifuge tubes) located within a glove box was used where indicated.

Anhydrous 1,3,5-trimethylbenzene (mesitylene) (98%), α,α,α-trifluorotoluene (≥99%), fluorobenzene (99%),

hexafluorobenzene (99%), 1,2-difluorobenzene (98%), 1,3-difluorobenzene (≥99%), and bromobenzene (99%) were purchased from Sigma-Aldrich. Hexanes, *n*-pentane, benzene, toluene and THF were purchased from Caledon, and deuterated solvents (C_6D_6, toluene-d_8, C_6D_5Br) were purchased from ACP Chemicals.

Hexanes, *n*-pentane, benzene and THF were initially dried and distilled at atmospheric pressure from sodium/benzophenone, while toluene was dried and distilled at atmospheric pressure from sodium. These solvents were then stored over an appropriate drying agent (toluene, benzene, THF = Na/Ph_2CO; hexanes, *n*-pentane = Na/Ph_2CO/tetraglyme) and introduced to reactions or solvent storage flasks *via* vacuum transfer with condensation at −78 °C. Mesitylene was dried and distilled under reduced pressure (<10 mTorr) from sodium/benzophenone, whereas α,α,α-trifluorotoluene, fluorobenzene, hexafluorobenzene, 1,2-difluorobenzene, and 1,3-difluorobenzene were dried and distilled at reduced pressure (<10 mTorr) from 4 Å molecular sieves. Bromobenzene was dried and distilled under reduced pressure (<10 mTorr) at elevated temperature (60 °C) from 4 Å molecular sieves. Deuterated solvents were dried over sodium/benzophenone (C_6D_6, toluene-d_8) or 4 Å molecular sieves (C_6D_5Br), and degassed *via* three freeze–pump–thaw cycles prior to distillation into a storage flask under a static vacuum.

$[Th(NO_3)_4(H_2O)_4]$, UO_3, and $[Ph_3C][B(C_6F_5)_4]$ (97%; used as received) were purchased from Strem Chemicals. Na, NaH, and $LiCH_2SiMe_3$ (1.0 M in *n*-pentane) were purchased from Sigma-Aldrich. Argon and ethylene of 99.999% purity were purchased from Praxair. Prior to use, solid $LiCH_2SiMe_3$ was obtained by removal of solvent *in vacuo*. Before use, all traces of moisture and ethanol were eliminated from $H_2(XA_2)$ by stirring with NaH (4 equiv.) in toluene for 16 hours at room temperature, followed by filtration and evaporation to dryness *in vacuo*. All dried/purified reagents were stored under vacuum or argon. $H_2(XA_2)$,[70] UCl_4,[71] $[(XA_2)ThCl_2(dme)]$,[70] $[(XA_2)Th(CH_2SiMe_3)_2]$ (**1-Th**),[70] $[(XA_2)UCl_3\{K(dme)_3\}]$, $[(XA_2)U(CH_2SiMe_3)_2]$[41] and KCH_2Ph[72] were prepared using literature procedures. $[ThCl_4(dme)_2]$ was prepared using two different methods: a modified version of the procedure reported by Gambarotta *et al.*,[73] and the procedure of Kiplinger *et al.* (at 50 °C).[74]

Nuclear magnetic resonance spectroscopy (^1H, ^2H, ^{19}F) experiments were performed on Bruker AV-200, DRX-500 and AV-600 spectrometers. Spectra were obtained at 298 K unless otherwise specified. ^1H NMR spectra are referenced relative to $SiMe_4$ through a resonance of the protio impurity of the solvent; C_6D_6 (δ 7.16 ppm), toluene-d_8 (δ 7.09, 7.01, 6.97, 2.08 ppm), C_6D_5Br (δ 7.30, 7.02, 6.94 ppm), cyclohexane-d_{12} (10%) in C_6H_5F or *o*-$C_6H_4F_2$ (δ 1.34 ppm). ^{19}F NMR spectra were referenced using an external standard of $CFCl_3$ (0.0 ppm). Herein, for XA_2, Aryl = 2,6-diisopropylphenyl. Peaks in the ^1H NMR spectra of paramagnetic uranium(IV) complexes were assigned primarily based on integration. Occasionally, the *para*-aryl, CH,[1,8] CH^3,[6] and *tert*-butyl signals could be readily identified as they are often unaffected by the presence/absence of top-bottom symmetry on the NMR timescale. Furthermore, the *para*-Ar signal often appeared as a triplet at room temperature, allowing definite assignment. For uranium alkyl complexes, significantly broadened ^1H NMR signals (typically integrating to approximately 2H) shifted to particularly low- or high- frequencies were speculatively assigned as the UCH_2 alpha-protons given their close proximity to the paramagnetic U(IV) centre.

X-ray crystallographic analyses were performed on suitable crystals coated in Paratone oil and mounted on a SMART APEX II diffractometer with a 3 kW Sealed tube Mo generator in the McMaster Analytical X-ray (MAX) Diffraction Facility. Crystal mounting, X-ray data collection at 100 K (**5** and **6**), 150 K (**2**), or 173 K (**3**), and structure solution and refinement were carried out by Dr Hilary Jenkins and Dr Jim Britten of the McMaster Analytical X-ray (MAX) Diffraction Facility. A semi-empirical absorption correction was applied using redundant data. Raw data was processed using XPREP (as part of the APEX2.2.0 software), and solved by direct (SHELX-97 or SHELXTL)[75] methods. The structures were completed by difference Fourier synthesis and refined with full-matrix least-squares procedures based on F^2. In all cases, non-hydrogen atoms were refined anisotropically (with the exception of carbon and oxygen atoms composing lattice solvent in **5** and **6**) and hydrogen atoms were generated in ideal positions and then updated with each cycle of refinement (with the exception of hydrogen atoms on C48 in **2** and **5**, which were located from the difference map and refined isotropically). Refinement was performed with SHELXL[76] using WinGX or Olex2.[77]

Combustion elemental analyses were performed on a Thermo EA1112 CHNS/O analyzer by Ms. Meghan Fair or Dr Steve Kornic at McMaster University, and on a Carlo Erba EA 1110 CHN elemental analyzer at Simon Fraser University by Mr Farzad Haftbaradaran, with sample preparation conducted by Dr Wen Zhou in the Leznoff group at Simon Fraser University.

Polyethylene samples were investigated by Differential Scanning Calorimetry (DSC) using a TA Instruments DSC Q20. Samples were measured between 40 and 180 °C using a heating and cooling rate of 10 °C min^{-1}; peak melting temperatures were obtained from the second of two heating runs.

Gel permeation chromatograms (GPCs) were recorded on an Agilent PL220 high temperature instrument equipped with differential refractive index (DRI) and viscometry (VS) detectors at the University of Warwick, Coventry, UK by Dr Daniel W. Lester and Dr Ian Hancox. The system was equipped with 2 × PLgel Mixed D columns (300 × 7.5 mm) and a PLgel 5 μm guard column. Samples were dissolved in 1,2,4-trichlorobenzene and left to solubilize for 12 h on an Agilent PL SP260VS at 140 °C, and all data was calibrated against polystyrene. The mobile phase was trichlorobenzene stabilized with 250 ppm BHT and run at a flow rate of 1 mL min^{-1} at 160 °C.

$[(XA_2)U(CH_2SiMe_3)(\eta^6\text{-}C_6H_6)][B(C_6F_5)_4]\cdot 2$ benzene. (**2**·2 C_6H_6). Solid $[Ph_3C][B(C_6F_5)_4]$ (0.079 g, 0.087 mmol) was quickly added to a stirring solution of $[(XA_2)U(CH_2SiMe_3)_2]\cdot(C_5H_{12})$ (**1**·C_5H_{12}) (0.100 g, 0.087 mmol) in benzene (10 mL) at room temperature. The bright red solution immediately darkened to a deep yellow-brown colour, and stirring was continued at room temperature for ∼1 hour. The deep brown solution was then layered with hexanes and cooled to −30 °C. After several days, X-ray quality deep brown crystals of **2**·2 C_6H_6 were collected,

washed with benzene and *n*-pentane, and dried *in vacuo* to provide 0.119 g of **2**·2 C_6H_6 (0.062 mmol, 72% yield). ^{1}H NMR (bromobenzene-d_5 + 100 equivalents of benzene-d_6, 500.1 MHz, 298 K): δ 79.47, 9.88 (broad s, 2 × 2H), 32.75, 32.52, 22.25, 19.69, −12.55 (s, 5 × 2H), 22.17, 17.28, 7.60, −7.39 (s, 4 × 6H, CH*Me*$_2$), 4.31 (s, 18H, CMe$_3$), −11.44, −16.64 (s, 2 × 3H, C*Me*$_2$), −12.13 (s, 9H, SiMe$_3$), −39.45 (v. broad s, 2H, UC*H*$_2$). The η^6-C_6H_6 resonance was observed at −29.43 ppm in the ^{1}H NMR spectrum of **2** in neat bromobenzene-d_5. Anal. Calcd for $C_{93}H_{91}N_2$-OSiUBF$_{20}$: C, 58.49; H, 4.80; N, 1.47%. Found: C, 58.62; H, 4.73; N, 1.22%. Conducting the alkyl abstraction reaction in benzene-d_6 followed by an identical work-up yielded the deuterobenzene isotopologue **2-*d*$_6$** in comparable yield. ^{2}H NMR (bromobenzene + 5 equivalents benzene-d_6, 92.1 MHz, 298 K): δ −29.84 (v broad s, 6D, η^6-C_6D_6).

[(XA$_2$)U(CH$_2$SiMe$_3$)(η^3-C$_6$H$_5$Me)][B(C$_6$F$_5$)$_4$]·2 toluene. (**3**·2 C_6H_5Me). The synthesis of **3**·2 C_6H_5Me was analogous to that of **2**·2 C_6H_6, using [Ph$_3$C][B(C$_6$F$_5$)$_4$] (0.099 g, 0.108 mmol) and [(XA$_2$)U(CH$_2$SiMe$_3$)$_2$]·C$_5$H$_{12}$ (0.125 g, 0.108 mmol) in toluene (10 mL). Crystalline **3**·2 C_6H_5Me was washed with toluene and *n*-pentane, and dried *in vacuo* to provide 0.172 g of **3**·2 C_6H_5Me (0.088 mmol, 81% yield). X-ray quality crystals of **3**·C_6H_5Me were grown from toluene/hexanes at −30 °C, and were additionally utilized for elemental analysis. ^{1}H NMR (bromobenzene-d_5 + 100 equivalents of toluene-d_8, 500.1 MHz, 298 K): δ 78.97, 10.59 (broad s, 2 × 2H), 32.84, 32.75, 22.33, 19.89, −12.57 (s, 5 × 2H), 22.26, 17.62, 7.60, −7.63 (s, 4 × 6H, CH*Me*$_2$), 4.32 (s, 18H, CMe$_3$), −11.42, −17.14 (s, 2 × 3H, C*Me*$_2$), −12.11 (s, 9H, SiMe$_3$), −37.16 (v. broad s, 2H, UC*H*$_2$). The η^3-C_6H_5Me resonances {−17.05, −22.63 (s, 2 × 2H, *o*/*m*-*Ph*Me), −19.20 (s, 3H, Ph*Me*), and −67.53 ppm (s, 1H, *p*-*Ph*Me)} were observed in the ^{1}H NMR spectrum of **3** in neat bromobenzene-d_5. Anal. Calcd for $C_{89}H_{89}N_2OSiUBF_{20}$: C, 57.48; H, 4.82; N, 1.51%. Found: C, 57.00; H, 4.81; N, 1.66%. Conducting the alkyl abstraction in toluene-d_8 followed by identical work-up yielded the deuterotoluene isotopologue **3**-d_8 in comparable yield. ^{2}H NMR (bromobenzene + 5 equivalents toluene-d_8, 92.1 MHz, 298 K): δ −17.53, −22.78 (m, 2 × 2D, *o*/*m*-C*D*), −19.28 (broad s, 3D, C*D*$_3$), −67.28 (m, 1D, *p*-C*D*).

[(XA$_2$)U(CH$_2$SiMe$_3$)(η^x-C$_6$D$_5$Br)][B(C$_6$F$_5$)$_4$]. (**4**-d_5; *in situ*) A sample (∼10 mg) of cation **2**, **3**, or **5** was taken up in ∼0.6 mL bromobenzene-d_5 to afford a deep brown solution. Five minutes after mixing, ^{1}H NMR spectroscopy revealed signals corresponding predominantly to **4-*d*$_5$**. Alternatively, cation **4-*d*$_5$** may be generated directly *via* the reaction of **1** with [Ph$_3$C][B(C$_6$F$_5$)$_4$] in C_6D_5Br. ^{1}H NMR (bromobenzene-d_5, 500.1 MHz, 298 K): δ 79.79, 9.72 (broad s, 2 × 2H), 32.95, 32.69, 22.35, 19.77, −12.61 (s, 5 × 2H), 22.28, 17.28, 7.63, −7.61 (s, 4 × 6H, CH*Me*$_2$), 4.33 (s, 18H, CMe$_3$), −11.46, −16.67 (s, 2 × 3H, C*Me*$_2$), −12.25 (s, 9H, SiMe$_3$), −40.76 (v broad s, 2H, UC*H*$_2$). ^{2}H NMR (bromobenzene-d_5, 92.1 MHz, 298 K): δ −29.20, −29.56 (η^x-C_6D_5Br). These two sharper peaks may overlap with a third broad singlet at −29 ppm.

[(XA$_2$)U(CH$_2$SiMe$_3$)(η^3-C$_6$H$_5$F)][B(C$_6$F$_5$)$_4$] (5). The synthesis of **5** was analogous to that of **2**·2 C_6H_6, using [Ph$_3$C][B(C$_6$F$_5$)$_4$] (0.079 g, 0.087 mmol) and [(XA$_2$)U(CH$_2$SiMe$_3$)$_2$]·C$_5$H$_{12}$ (0.100 g, 0.087 mmol) in fluorobenzene (10 mL). After 30 minutes, the brown solution was evaporated to dryness, yielding a deep brown residue which was redissolved in a minimum amount of fluorobenzene (∼1 mL), layered with *n*-pentane, and cooled to −30 °C. After several days, deep brown microcrystalline **5**·C_6H_5F was collected, washed with *n*-pentane (3 × 5 mL), and dried *in vacuo* to provide 0.140 g of **5** (0.079 mmol, 91% yield). X-ray quality crystals of **5**·C_6H_5F were grown from fluorobenzene/*n*-pentane at −30 °C. ^{1}H NMR (bromobenzene-d_5, 600.1 MHz, 298 K) : cation **5** is readily converted to C_6D_5Br-bound cation **4-*d*$_5$** in bromobenzene-d_5, therefore the ^{1}H NMR spectrum in this solvent is identical to that of **4-*d*$_5$**, but containing one equivalent of free fluorobenzene. ^{1}H NMR (fluorobenzene + 10% cyclohexane-d_{12}, 600.1 MHz, 298 K): 37.14, 20.65, −13.09 (s, 3 × 2H, C*H*,[1,8] C*H*,[3,6] aryl-*para* C*H*), 4.95 (s, 18H, C*Me*$_3$), −14.13 (s, 9H, Si*Me*$_3$), −59.34 (broad s, 2H, UC*H*$_2$). ^{1}H NMR (fluorobenzene + 10% cyclohexane-d_{12}, 600.1 MHz, 237 K): 106.24 (broad s, 2H), 46.26, 24.70, −17.95 (s, 3 × 2H, C*H*,[1,8] C*H*,[3,6] aryl-*para* C*H*), 44.48, 28.26, 5.34 (s, 3 × 2H, C*H*Me$_2$, aryl-*meta* C*H*), 31.61, 21.42, 9.85, −20.06 (s, 4 × 6H, CH*Me*$_2$), 6.08 (s, 18H, C*Me*$_3$), −15.46, −22.88 (s, 2 × 3H, C*Me*$_2$), −18.47 (s, 9H, Si*Me*$_3$), −90.98 (broad s, 2H, UC*H*$_2$). ^{19}F{^{1}H} NMR (fluorobenzene + 10% cyclohexane-d_{12}, 188.2 MHz, 298 K): δ −113.38 (s, free C_6H_5F), −134.18 (broad s, 8F, *o*-C$_6$*F*$_5$), −165.19 (t, $^3J_{19F-19F}$ = 21 Hz, 4F, *p*-C$_6$*F*$_5$), −169.01 (broad t, $^3J_{19F-19F}$ = 19 Hz, 8F, *m*-C$_6$*F*$_5$); signals for coordinated fluorobenzene were not observed between +1200 and −1200 ppm at 25 or −35 °C. Anal. Calcd for $C_{81}H_{78}$-$N_2OSiUBF_{21}$: C, 54.92; H, 4.44; N, 1.58%. Found: C, 54.96; H, 4.61; N, 1.55%.

***In situ* reaction of 1-Th with [Ph$_3$C][B(C$_6$F$_5$)$_4$] in C$_6$H$_5$F.** Solid [Ph$_3$C][B(C$_6$F$_5$)$_4$] (0.005 g, 0.005 mmol) was added quickly to a stirring solution of [(XA$_2$)Th(CH$_2$SiMe$_3$)$_2$]·0.5{O(SiMe$_3$)$_2$} (**1-Th** 0.5{O(SiMe$_3$)$_2$}) (0.006 g, 0.005 mmol) in fluorobenzene (5 mL) at room temperature. The colourless solution immediately became a bright yellow-orange colour, and stirring was continued at room temperature for ∼3.5 or 24 h. This vibrant orange solution, presumably containing [(XA$_2$)Th(CH$_2$SiMe$_3$)(η^x-C_6H_5F)][B(C$_6$F$_5$)$_4$] (**5-Th**; the thorium analogue of **5**) was then utilized directly for ethylene polymerization trials.

***In situ* reaction of 1 with [Ph$_3$C][B(C$_6$F$_5$)$_4$] in *o*-C$_6$H$_4$F$_2$.** Solid [Ph$_3$C][B(C$_6$F$_5$)$_4$] (0.008 g, 0.0087 mmol) was added quickly to a stirring solution of [(XA$_2$)U(CH$_2$SiMe$_3$)$_2$]·C$_5$H$_{12}$ (**1**·C$_5$H$_{12}$) (0.010 g, 0.0087 mmol) in *o*-difluorobenzene (0.7 mL) and cyclohexane-d_{12} (0.1 mL) at room temperature. The orange-red solution immediately became a deep yellow-brown colour, and stirring was continued at room temperature for 5 minutes. A ^{1}H NMR spectrum taken approximately 1.5 h after mixing revealed a collection of broad resonances accompanied by ∼30% unreacted **1** as well as numerous low intensity signals arising from unidentified paramagnetic decomposition products. After 24 h at room temperature, ∼10% unreacted **1** remained in solution, and appreciable $SiMe_4$ evolution indicated that the reaction product suffers from poor thermal stability. ^{1}H NMR of the major paramagnetic reaction product (*o*-$C_6H_4F_2$ + 10% cyclohexane-d_{12}, 600.1 MHz, 298 K; selected resonances): 42.81, 20.80, 5.87, 4.46, −12.29, −12.79, −16.51 (broad s × 7). ^{19}F{^{1}H} NMR (*o*-$C_6H_4F_2$ + 10% cyclohexane-d_{12}, 188.2 MHz, 298 K): δ −133.04 (broad s, 8F, *o*-C$_6$*F*$_5$), −139.66 (s, free *o*-C$_6$H$_4$*F*$_2$),

−165.09 (t, $^3J_{19F-19F} = 20$ Hz, 4F, *p*-C_6F_5), −168.85 (broad t, $^3J_{19F-19F} = 18$ Hz, 8F, *m*-C_6F_5).

[$(XA_2)U(CH_2Ph)_2$] (6). A mixture of [$(XA_2)UCl_3${K(dme)$_3$}] (0.200 g, 0.15 mmol) and 2 equiv. of KCH_2Ph (0.039 g, 0.30 mmol) in diethylether (30 mL) was stirred initially at −94 °C, then at −78 °C, before warming slowly to room temperature; stirring was continued for a total of 12 h. The deep-brown solution was evaporated to dryness *in vacuo*, and the solid residue was extracted with a minimum amount of hexanes (∼11 mL). The suspension was centrifuged to remove insoluble KCl, and the deep-brown mother liquors were evaporated to dryness *in vacuo*, yielding an iridescent blackish solid residue. The solids were dissolved in minimal *n*-pentane (∼8 mL) and cooled to −30 °C. Black crystalline **6** was collected after several days, the mother liquors were returned to the freezer, and another crop of crystalline **6** was collected after a few days. The crystals were dried *in vacuo* to provide 0.123 g of **6** (0.112 mmol, 74% yield). Alternatively, the reaction was conducted in THF; after identical workup and crystallization from minimal hexanes at −30 °C, X-ray quality crystals of **6**·THF were obtained. ^{1}H NMR (toluene-d_8, 500.1 MHz, 298 K): δ 100.92, 61.75 (v. broad s, 2 × 2H, UCH_2), 51.04, 18.59, 12.90, −4.30, −8.34, −13.85 (v. broad s, 6 × 2H, Aryl-*meta* CH {× 2}, benzyl-*ortho* CH {× 2}, benzyl-*meta* CH {× 2}), 41.07, −62.32 (v. broad s, 2 × 2H, C*H*Me$_2$), 34.47, 1.25, −5.95, −7.19 (v. broad s, 4 × 6H, CH*Me*$_2$), 9.36, −12.38 (v. broad s, 2 × 1H, benzyl-*para* CH), 4.59 (t, $^3J_{H,H} = 6$ Hz, 2H, aryl-*para* CH), 0.85, −5.17 (v. broad s, 2 × 3H, C*Me*$_2$), −2.20, −13.46 (s, 2 × 2H, CH^{1,8} and CH^{3,6}), −3.08 (s, 18H, CMe$_3$). ^{1}H NMR (toluene-d_8, 500.1 MHz, 262 K): δ 124.45, 82.22 (v. broad s, 2 × 2H, UCH_2), 55.18, 21.28, 13.94, −6.98, −11.61, −18.58 (broad s, 6 × 2H, aryl-*meta* CH {× 2}, benzyl-*ortho* CH {× 2}, benzyl-*meta* CH {× 2}), 49.38, −72.24 (broad s, 2 × 2H, C*H*Me$_2$), 41.30, 0.40, −7.66, −9.17 (broad s, 4 × 6H, CH*Me*$_2$), 11.19, −15.72 (broad s, 2 × 1H, benzyl-*para* CH), 4.06 (broad s, 2H, aryl-*para* CH), 2.89, −5.90 (broad s, 2 × 3H, C*Me*$_2$), −3.04, −17.67 (broad s, 2 × 2H, CH^{1,8} and CH^{3,6}), −3.94 (s, 18H, CMe$_3$). Anal. Calcd for $C_{61}H_{76}N_2OU$: C, 67.14; H, 7.02; N, 2.57%. Found: C, 67.22; H, 7.23; N, 2.67%.

Ethylene polymerization. The appropriate actinide(IV) dialkyl precursor (0.005 mmol, < 10 mg) was dissolved in 4–5 mL of deoxygenated, anhydrous solvent in a 25 mL round bottomed flask in the glovebox. For reactions where cationic species were generated *in situ* utilizing [Ph_3C][$B(C_6F_5)_4$] as an activating agent, the trityl salt (0.005 g, 0.005 mmol) was added as a solid to the stirring precursor solution (accompanied by a rapid colour change in aromatic solvents). For reactions where An = U, the solution was allowed to stir for 30 minutes (in C_6H_6, C_6H_5Me, C_6H_5Br, or *o*-$C_6H_4F_2$), 3.5 hours (in C_6H_5F), or 24 hours {in alkane solvents under ethylene (1 atm), with our without 3 equiv. of added toluene or fluorobenzene}. Note: (a) for the reactions of **1** in C_6H_5F, higher activities were observed after activation for 3.5 hours *vs.* 30 minutes, and (b) for reactions of **1-Th** in C_6H_5F, near identical activities were observed after activation for 3.5 hours *vs.* 24 hours. Once activated, the solution was degassed, and dynamic ethylene (1 atm) was admitted; for reactions conducted at elevated temperature, the mixture was heated to 70 °C prior to introducing ethylene. After 5 or 30 min (in arene solvents) or 24 h (in alkane solvents), the reaction was quenched by venting the ethylene that remained in the headspace and adding ∼5−7 mL of acidified methanol (10 vol% conc. hydrochloric acid in methanol). The precipitated polymer solids were collected on a fritted glass funnel, washed with methanol, and dried *in vacuo*.

DFT calculations. All calculated structures were fully optimized with the ADF/AMS DFT package (SCM, version 2020.102).[78,79] Calculations were conducted in the gas phase within the generalized gradient approximation using the 1996 Perdew–Burke–Ernzerhof exchange and correlation functional (PBE),[80] the scalar zeroth-order regular approximation (ZORA)[81–85] for relativistic effects, and Grimme's DFT-D3-BJ dispersion correction.[86,87] Geometry optimizations were conducted using all-electron (without frozen cores) triple-ζ basis sets with two polarization functions (TZ2P), fine integration grids (Becke[88,89] very good), stricter-than-default convergence criteria (gradients = 0.0001, step = 0.002), a charge of +1, and C_s symmetry {except **5b′**, or during geometry optimization of fragments (for calculation of ΔE_{prep}), for which no symmetry was enforced}. Calculations for **2′-Th** were restricted, whereas those for **2′**, **3′**, **5′**, **5a′**, and **5b′** (or uranium-containing fragments) were unrestricted with a net spin polarization of 2.

Visualization of the computational results was performed using the ADF/AMS-GUI (SCM) or Biovia Discovery Studio Visualizer. Orbitals and deformation densities were generated with a fine grid using the densf auxiliary program.

Analytical frequency calculations[90–92] were conducted on all geometry optimized structures (including geometry optimized fragments) to ensure that the geometry optimization led to an energy minimum or (when using C_s symmetry) a situation where any imaginary frequency corresponds to a breaking of the symmetry; for **2′**, **2′-Th**, **3′**, and **5′**, imaginary frequencies were obtained (ranging from −52 to −8 cm^{-1}, with intensities ≤ 0.4 km^{-mol}) corresponding to rotations which also would break the C_s symmetry. Analytical frequency calculations were also used to obtain thermodynamic parameters for **5′**, **5a′**, and **5b′**.

Bonding was analyzed in more detail using a fragment approach (with energy decomposition analysis[62,63] and ETS-NOCV analysis[64–67]) that considered the interaction of cationic $(XA_{2'})An(CH_2SiMe_3)^+$ fragments with neutral arene ligands (fragments were generated from the TZ2P geometry optimized structures of each complex, and geometries were frozen). The thresholds for (a) population analysis of each deformation density contribution in terms of individual SFO's, (b) orbital interaction energy contributions corresponding to deformation density components originating from each NOCV-pair, and (c) NOCV eigenvalues were lowered to 0.001, 1, and 0.03, respectively. Fragment interaction calculations involving uranium were conducted using the unrestricted fragments method. Preparation energies (ΔE_{prep}) were obtained by allowing the fragments to adopt equilibrium geometries (*i.e.* geometry optimized, without imposed symmetry). Basis set superposition errors (BSSEs) were calculated through the use of ghost atoms with no nuclear charge and no electrons to contribute to the molecule (using the molecular fragments method).

Data availability

All relevant experimental data is included as ESI.‡

Author contributions

Nicholas R. Andreychuk: investigation, visualization, writing – original draft, review & editing. Balamurugan Vidjayacoumar: investigation. Jeffrey S. Price: formal analysis, investigation, visualization, writing – original draft, review & editing. Sophie Kervazo: formal analysis, investigation, visualization. Craig A. Peeples: formal analysis, investigation. David J. H. Emslie: conceptualization, funding acquisition, project administration, supervision, writing – original draft, review & editing. Valérie Vallet: formal analysis, investigation, funding acquisition, project administration, resources, supervision, visualization. André S. P. Gomes & Florent Réal: funding acquisition, resources, supervision. Georg Schreckenbach: funding acquisition, supervision, writing – review & editing. Paul W. Ayers: funding acquisition, supervision, writing – review & editing. Ignacio Vargas-Baca: supervision, writing – review & editing. Hilary A. Jenkins & James F. Britten: formal analysis.

Conflicts of interest

There are no conflicts to declare.

Acknowledgements

D. J. H. E. and G. S. thank NSERC of Canada for a Discovery Grant, and D. J. H. E. thanks the Digital Research Alliance of Canada (previously Compute Canada) for a 2020 Resources for Research Groups (RRG) grant. P. W. A. thanks NSERC, Digital Research Alliance of Canada, and the Canada Research Chairs for funding and computational resources. S. K., V. V., A. S. P. G. and F. R. acknowledge funding Labex CaPPA (Grant No ANR-11-LABX-0005-01). N. R. A. thanks the Government of Ontario for an Ontario Graduate Scholarship (OGS), and McMaster University for a Richard Fuller Memorial Scholarship. We are very grateful to Dr Wen Zhou in the Leznoff group at Simon Fraser University for preparing and submitting Elemental Analysis samples on our behalf.

Notes and references

§ When generated *in situ* in benzene or toluene, compounds **2** and **3** remained in solution, at least on a timescale of hours. However, solid samples of **2**·2 benzene and **3**·x toluene ($x = 1$ or 2) were very poorly soluble in benzene or toluene (*i.e.* they could not readily be re-dissolved).

¶ The reaction of **1** with $[Ph_3C][B(C_6F_5)_4]$ in 1,3-difluorobenzene yielded a yellow-brown solution; the analogous reactions in mesitylene, C_6F_6, and α,α,α-trifluorotoluene yielded oily black-brown, brown, or black-green precipitates, respectively. In contrast, reaction of a dark green-brown solution of $[(XA_2)U(CH_2Ph)_2]$ (**7**) with $[Ph_3C][B(C_6F_5)_4]$ in C_6H_5F afforded a yellow-brown solution.

‖ The deformation density contributions ($\Delta\rho_n$) obtained from ETS-NOCV calculations are numbered (n) based on qualitative analysis of the deformation density isosurfaces.

1 A. A. Trifonov and D. M. Lyubov, *Coord. Chem. Rev.*, 2017, **340**, 10.
2 D. Peng, X. Yan, C. Yu, S. Zhang and X. Li, *Polymer Chemistry*, 2016, **7**, 2601.
3 A. A. Altaf, A. Badshah, N. Khan, S. Marwat and S. Ali, *J. Coord. Chem.*, 2011, **64**, 1815.
4 I. D. Burdett and R. S. Eisinger, in *Handbook of Industrial Polyethylene and Technology: Definitive Guide to Manufacturing, Properties, Processing, Applications and Markets*, ed. M. A. Spalding and A. M. Chatterjee, Scrivener Publishing, Beverly, MA, 2018, ch. 3, p. 61.
5 J. M. Asua, *Polymer Reaction Engineering*, Blackwell Publishing, Ames, Iowa, 2007.
6 A. Peacock and A. Calhoun, *Polymer Chemistry: Properties and Applications*, Carl Hanser Verlag, Munich, 2006.
7 D. Malpass, *Introduction to Industrial Polyethylene: Properties, Catalysts and Processes*, Wiley-Scrivener, Hoboken, 2010.
8 S. J. Lancaster, O. B. Robinson, M. Bochmann, S. J. Coles and M. B. Hursthouse, *Organometallics*, 1995, **14**, 2456.
9 D. J. Gillis, M.-J. Tudoret and M. C. Baird, *J. Am. Chem. Soc.*, 1993, **115**, 2543.
10 D. J. Gillis, R. Quyoum, M.-J. Tudoret, Q. Wang, D. Jeremic, A. W. Roszak and M. C. Baird, *Organometallics*, 1996, **15**, 3600.
11 C. Pellecchia, A. Proto, P. Longo and A. Zambelli, *Makromolekulare Chemie-Rapid Communications*, 1992, **13**, 277.
12 Q. Wang, R. Quyoum, D. J. Gillis, M.-J. Tudoret, D. Jeremic, B. K. Hunter and M. C. Baird, *Organometallics*, 1996, **15**, 693.
13 P. G. Hayes, W. E. Piers and M. Parvez, *J. Am. Chem. Soc.*, 2003, **125**, 5622.
14 P. G. Hayes, W. E. Piers and M. Parvez, *Chem. Eur. J.*, 2007, **13**, 2632.
15 J. D. Scollard, D. H. McConville, N. C. Payne and J. J. Vittal, *Macromolecules*, 1996, **29**, 5241.
16 J. D. Scollard and D. H. McConville, *J. Am. Chem. Soc.*, 1996, **118**, 10008.
17 Y.-X. Chen and T. J. Marks, *Organometallics*, 1997, **16**, 3649.
18 K. S. A. Motolko, J. S. Price, D. J. H. Emslie, H. A. Jenkins and J. F. Britten, *Organometallics*, 2017, **36**, 3084.
19 C. A. Cruz, D. J. H. Emslie, C. M. Robertson, L. E. Harrington, H. A. Jenkins and J. F. Britten, *Organometallics*, 2009, **28**, 1891.
20 Sadow *et al.* also recently reported toluene-coordinated $[Nd\{C(SiHMe_2)_3\}\{\eta^6\text{-toluene}\}\{HB(C_6F_5)_3\}_2]$ which can be viewed as an neodymium alkyl dication with tight coordination of two $HB(C_6F_5)_3$– anions: B. M. Schmidt, A. Pindwal, A. Venkatesh, A. Ellern, A. J. Rossini and A. D. Sadow, *ACS Catal.*, 2019, **9**, 827.
21 C. A. Cruz, D. J. H. Emslie, L. E. Harrington and J. F. Britten, *Organometallics*, 2008, **27**, 15.
22 M. Bochmann, G. Karger and A. J. Jaggar, *J. Chem. Soc. Chem. Commun.*, 1990, 1038.
23 A. D. Horton and J. H. G. Frijns, *Angew. Chem., Int. Ed. Engl.*, 1991, **30**, 1152.
24 M. Bochmann and A. J. Jaggar, *J. Organomet. Chem.*, 1992, **424**, C5.

25 M. Bochmann, *Angew. Chem., Int. Ed. Engl.*, 1992, **31**, 1181.
26 G. G. Hlatky, H. W. Turner and R. R. Eckman, *J. Am. Chem. Soc.*, 1989, **111**, 2728.
27 B.-T. Guan, B. L. Wang, M. Nishiura and Z. M. Hou, *Angew. Chem., Int. Ed.*, 2013, **52**, 4418.
28 T. Li, M. Nishiura, J. Cheng, W. Zhang, Y. Li and Z. Hou, *Organometallics*, 2013, **32**, 4142.
29 D. J. H. Emslie, N. R. Andreychuk and C. A. Cruz, in *The Lanthanides and Actinides: Synthesis, Reactivity, Properties and Applications*, ed. S. T. Liddle, D. P. Mills and L. S. Natrajan, World Scientific Publishing Co., 2022, ch. 7, p. 311.
30 L. Jia, X. Yang, C. L. Stern and T. J. Marks, *Organometallics*, 1997, **16**, 842.
31 Y.-X. Chen, C. L. Stern, S. Yang and T. J. Marks, *J. Am. Chem. Soc.*, 1996, **118**, 12451.
32 L. Jia, X. Yang, C. Stern and T. J. Marks, *Organometallics*, 1994, **13**, 3755.
33 X. Yang, W. A. King, M. Sabat and T. J. Marks, *Organometallics*, 1993, **12**, 4254.
34 X. Yang, C. L. Stern and T. J. Marks, *Organometallics*, 1991, **10**, 840.
35 Z. Lin, J.-F. Le Marechal, M. Sabat and T. J. Marks, *J. Am. Chem. Soc.*, 1987, **109**, 4127.
36 Y. X. Chen, M. V. Metz, L. T. Li, C. L. Stern and T. J. Marks, *J. Am. Chem. Soc.*, 1998, **120**, 6287.
37 See for example:(*a*) T. J. Marks, L. Ja and X. Yang, *U.S. Pat.*, 5477895, 1995; (*b*) T. J. Marks and Y.-X. Chen, *U.S. Pat.*, 6229034B1, 2001; (*c*) T. J. Marks and Y.-X. Chen, *U.S. Pat.*, 6274752B1, 2001; (*d*) T. J. Marks and Y.-X. Chen, *U.S. Pat.*, 6403732B2, 2002; (*e*) T. J. Marks and Y.-X. Chen, *U.S. Pat.*, 6388114B1, 2002; (*f*) R. E. Campbell Jr., *U.S. Pat.*, 4665046, 1987.
38 Isoprene polymerization catalysts generated *in situ* by reaction of non-carbocyclic thorium trialkyl complexes with 2 equiv. of $[CPh_3][B(C_6F_5)_4]$ (in the presence of $AliBu_3$) have also been reported: G. R. Qin and J. H. Cheng, *Dalton Trans.*, 2019, **48**, 11706.
39 E. Domeshek, R. J. Batrice, S. Aharonovich, B. Tumanskii, M. Botoshansky and M. S. Eisen, *Dalton Trans.*, 2013, **42**, 9069.
40 C. E. Hayes and D. B. Leznoff, *Organometallics*, 2010, **29**, 767.
41 N. R. Andreychuk, S. Ilango, B. Vidjayacoumar, D. J. H. Emslie and H. A. Jenkins, *Organometallics*, 2013, **32**, 1466.
42 R. D. Shannon, *Acta Cryst*, 1976, **A32**, 751.
43 L. Turculet and T. D. Tilley, *Organometallics*, 2002, **21**, 3961.
44 W. J. Evans, S. A. Kozimor and J. W. Ziller, *Organometallics*, 2005, **24**, 3407.
45 H. M. Dietrich, J. W. Ziller, R. Anwander and W. J. Evans, *Organometallics*, 2009, **28**, 1173.
46 M. J. Monreal and P. L. Diaconescu, *Organometallics*, 2008, **27**, 1702.
47 A cationic thorium aryl complex, $[Cp^*_2ThPh(THF)][BPh_4]$, has also been reported: R. R. Langeslay, C. J. Windorff, M. T. Dumas, J. W. Ziller and W. J. Evans, *Organometallics*, 2018, **37**, 454.
48 G. C. Campbell, F. A. Cotton, J. F. Haw and W. Schwotzer, *Organometallics*, 1986, **5**, 274.
49 F. A. Cotton and W. Schwotzer, *Organometallics*, 1985, **4**, 942.
50 B. Cordero, V. Gómez, A. E. Platero-Prats, M. Revés, J. Echeverría, E. Cremades, F. Barragán and S. Alvarez, *Dalton Trans.*, 2008, 2832.
51 S. Alvarez, *Dalton Trans.*, 2013, **42**, 8617.
52 G. Portalone, G. Schultz, A. Domenicano and I. Hargittai, *J. Mol. Struct.*, 1984, **118**, 53.
53 L. Pauling, *The Nature of the Chemical Bond*, Cornell University Press, New York, 3rd edn, 1960.
54 M. Mantina, A. C. Chamberlin, R. Valero, C. J. Cramer and D. G. Truhlar, *J. Phys. Chem. A*, 2009, **113**, 5806.
55 See for example:(*a*) A. Prades, M. Fernandez, S. D. Pike, M. C. Willis and A. S. Weller, *Angew. Chem., Int. Ed.*, 2015, **54**, 8520; (*b*) S. D. Pike, I. Pernik, R. Theron, J. S. McIndoe and A. S. Weller, *J. Organomet. Chem.*, 2015, **784**, 75; (*c*) H. Lei, J. C. Fettinger and P. P. Power, *Inorg. Chem.*, 2012, **51**, 1821; (*d*) A. K. Renfrew, A. D. Phillips, E. Tapavicza, R. Scopelliti, U. Rothlisberger and P. J. Dyson, *Organometallics*, 2009, **28**, 5061; (*e*) A. B. Chaplin and A. S. Weller, *Organometallics*, 2010, **29**, 2332; (*f*) T. B. Ditri, A. E. Carpenter, D. S. Ripatti, C. E. Moore, A. L. Rheingold and J. S. Figueroa, *Inorg. Chem.*, 2013, **52**, 13216; (*g*) M. M. D. Roy, M. J. Ferguson, R. McDonald and E. Rivard, *Chem. Commun.*, 2018, **54**, 483; (*h*) A. Friedrich, J. Eyselein, J. Langer and S. Harder, *Organometallics*, 2021, **40**, 448.
56 M. W. Bouwkamp, J. de Wolf, I. D. Morales, J. Gercama, A. Meetsma, S. I. Troyanov, B. Hessen and J. H. Teuben, *J. Am. Chem. Soc.*, 2002, **124**, 12956.
57 M. W. Bouwkamp, P. H. M. Budzelaar, J. Gercama, I. Del Hierro Morales, J. M. de Wolf, A. S. I. Troyanov, J. H. Teuben and B. Hessen, *J. Am. Chem. Soc.*, 2005, **127**, 14310.
58 F. Basuli, H. Aneetha, J. C. Huffman and D. J. Mindiola, *J. Am. Chem. Soc.*, 2005, **127**, 17992.
59 C. H. Lee, Y. H. La and J. W. Park, *Organometallics*, 2000, **19**, 344.
60 A. J. Bridgeman, G. Cavigliasso, L. R. Ireland and J. Rothery, *J. Chem. Soc., Dalton Trans.*, 2001, 2095.
61 F. M. Bickelhaupt and E. J. Baerends, in *Reviews in Computational Chemistry*, ed. K. B. Lipkowitz and D. B. Boyd, Wiley-VCH, New York, 2000, vol. 15, pp. 1.
62 T. Ziegler and A. Rauk, *Inorg. Chem.*, 1979, **18**, 1755.
63 T. Ziegler and A. Rauk, *Inorg. Chem.*, 1979, **18**, 1558.
64 M. Mitoraj and A. Michalak, *Organometallics*, 2007, **26**, 6576.
65 A. Michalak, M. Mitoraj and T. Ziegler, *J. Phys. Chem. A*, 2008, **112**, 1933.
66 M. P. Mitoraj, A. Michalak and T. Ziegler, *Organometallics*, 2009, **28**, 3727.
67 M. P. Mitoraj, A. Michalak and T. Ziegler, *J. Chem. Theory Comput.*, 2009, **5**, 962.
68 V. C. Gibson and S. K. Spitzmesser, *Chem. Rev.*, 2003, **103**, 283.
69 B. J. Burger and J. E. Bercaw, *Experimental Organometallic Chemistry – A Practicum in Synthesis and Characterization*,

American Chemical Society, Washington D.C., 1987, vol. 357, p. 79.
70 C. A. Cruz, D. J. H. Emslie, L. E. Harrington, J. F. Britten and C. M. Robertson, *Organometallics*, 2007, **26**, 692.
71 J. L. Kiplinger, D. E. Morris, B. L. Scott and C. J. Burns, *Organometallics*, 2002, **21**, 5978.
72 P. L. Bailey, R. A. Coxall, C. M. Dick, S. Fabre, L. C. Henderson, C. Herber, S. T. Liddle, D. Lorono-Gonzalez, A. Parkin and S. Parsons, *Chem. Eur. J.*, 2003, **9**, 4820.
73 A. Athimoolam, S. Gambarotta and I. Korobkov, *Organometallics*, 2005, **24**, 1996.
74 T. Cantat, B. L. Scott and J. L. Kiplinger, *Chem. Commun.*, 2010, **46**, 919.
75 G. M. Sheldrick, *Acta Crystallogr., Sect. A: Found. Crystallogr.*, 2008, **64**, 112.
76 G. M. Sheldrick, *Acta Crystallogr., Sect. C: Struct. Chem.*, 2015, **71**, 3.
77 O. V. Dolomanov, L. J. Bourhis, R. J. Gildea, J. A. K. Howard and H. Puschmann, *J. Appl. Crystallogr.*, 2009, **42**, 339.
78 *ADF 2020.102, SCM, Theoretical Chemistry*, Vrije Universiteit, Amsterdam, The Netherlands, **https://www.scm.com**.
79 G. Te Velde, F. M. Bickelhaupt, E. J. Baerends, C. Fonseca Guerra, S. J. A. Van Gisbergen, J. G. Snijders and T. Ziegler, *J. Comput. Chem.*, 2001, **22**, 931.
80 J. P. Perdew, K. Burke and M. Ernzerhof, *Phys. Rev. Lett.*, 1996, **77**, 3865.
81 E. van Lenthe, E. J. Baerends and J. G. Snijders, *J. Chem. Phys.*, 1993, **99**, 4597.
82 E. van Lenthe, E. J. Baerends and J. G. Snijders, *J. Chem. Phys.*, 1994, **101**, 9783.
83 E. van Lenthe, A. Ehlers and E.-J. Baerends, *J. Chem. Phys.*, 1999, **110**, 8943.
84 E. van Lenthe, J. G. Snijders and E. J. Baerends, *J. Chem. Phys.*, 1996, **105**, 6505.
85 E. van Lenthe, R. van Leeuwen, E. J. Baerends and J. G. Snijders, *Int. J. Quantum Chem.*, 1996, **57**, 281.
86 S. Grimme, J. Anthony, S. Ehrlich and H. Krieg, *J. Chem. Phys.*, 2010, **132**, 154104.
87 S. Grimme, S. Ehrlich and L. Goerigk, *J. Comput. Chem.*, 2011, **32**, 1456.
88 A. D. Becke, *J. Chem. Phys.*, 1988, **88**, 2547.
89 M. Franchini, P. H. T. Philipsen and L. Visscher, *J. Comput. Chem.*, 2013, **34**, 1819.
90 A. Bérces, R. M. Dickson, L. Y. Fan, H. Jacobsen, D. Swerhone and T. Ziegler, *Comput. Phys. Commun.*, 1997, **100**, 247.
91 H. Jacobsen, A. Bérces, D. P. Swerhone and T. Ziegler, *Comput. Phys. Commun.*, 1997, **100**, 263.
92 S. K. Wolff, *Int. J. Quantum Chem.*, 2005, **104**, 645.